Schweizerische Eidgenossenschaft
Confédération suisse
Confederazione Svizzera
Confederaziun svizra

Federal Department of the Environment, Transport, Energy and Communications DETEC

Swiss Federal Office of Energy SFOE
Energy Research and Cleantech Division

Final report dated 19.06.2025

ACIGS

Advancements in highly efficient CIGS photovoltaics

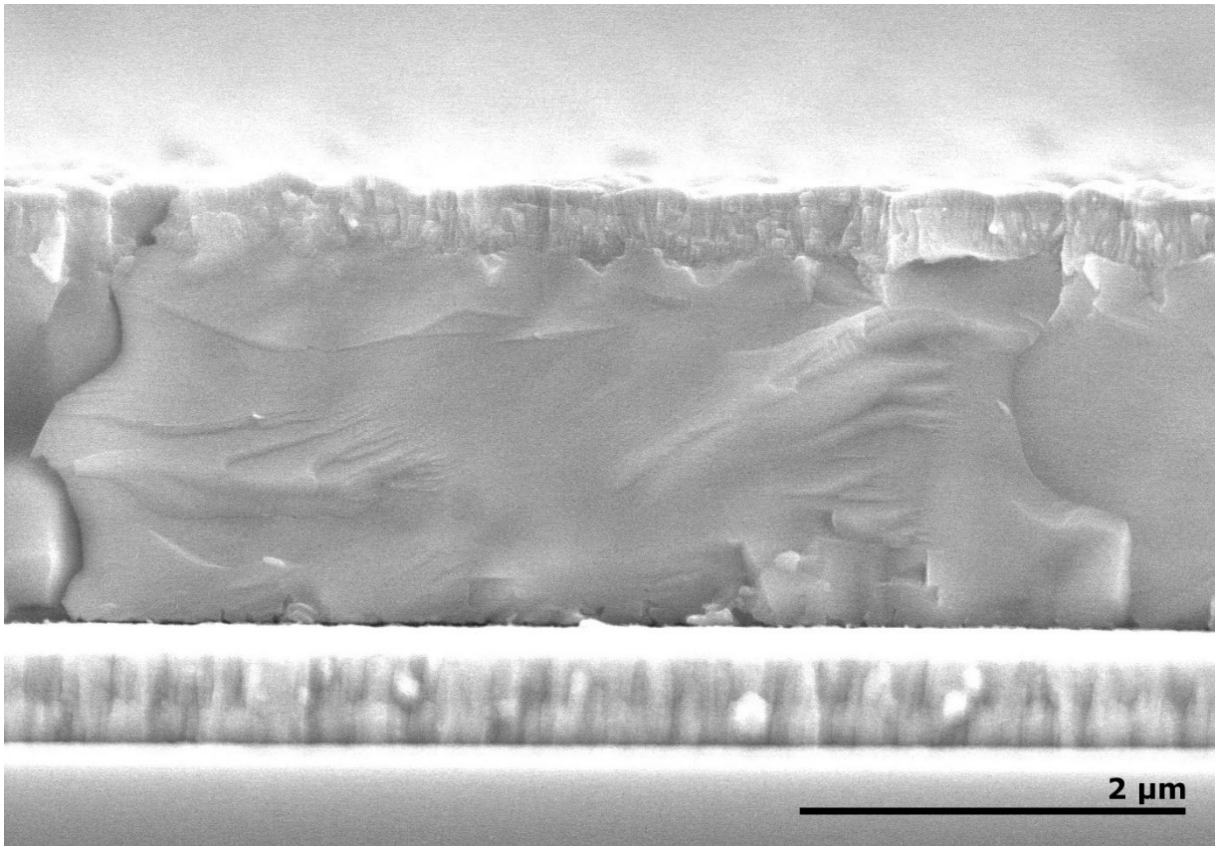

Source: ©Empa 2021

Empa
Materials Science and Technology

Date: 19 June 2025

Location: Bern

Publisher:
Swiss Federal Office of Energy SFOE
Energy Research and Cleantech
CH-3003 Bern
www.bfe.admin.ch

Subsidy recipients:
Empa
Laboratory for Thin Films and Photovoltaics
Ueberlandstrasse 129
8600 Dübendorf
www.empa.ch

Authors:
Romain Carron, Empa, romain.carron@empa.ch
Shiro Nishiwaki, Empa, shiro.nishiwaki@empa.ch
Matteo de Marzi, Empa, matteo.demarzi@empa.ch

SFOE project coordinators:
Stefan Oberholzer, Stefan.oberholzer@bfe.admin.ch

SFOE contract number: SI/502310-01

Zusammenfassung

Die Empa hat ein Herstellungsverfahren für flexible Cu(In,Ga)Se2 (CIGS) Solarzellen und -module auf Polymerfolien entwickelt. Die Komplexität des Prozesses und die engen Parameterfenster führen jedoch zu einer Kluft zwischen den Wirkungsgraden der Geräte im Labor und in der Industrie. Das Projekt zielt darauf ab, dieses Problem durch die Entwicklung eines neuen Prozesses für CIGS auf Polymerfolie zu lösen, der einfacher, leichter zu kontrollieren und robuster ist und gleichzeitig die zuvor gezeigten hohen Leistungen beibehält oder verbessert.

Der gewählte Legierungsansatz lieferte hervorragende Ergebnisse mit bereits winzigen Ag-Anteilen von etwa 2 % gegenüber Cu (0,5 % insgesamt). Wir haben eine extern zertifizierte Rekord-CIGS-Solarzelle auf flexiblen Polyimid-Substraten mit einem Wirkungsgrad von 22,2 % demonstriert. Ag kann als Vorläuferschicht oder durch verschiedene Varianten der Co-Verdampfung mit einer ähnlichen Wirkungsgradverbesserung von 0,5-1 % eingebracht werden, so dass beide Optionen für die industrielle Umsetzung offen stehen. Im Vergleich zu Ag-freien Zusammensetzungen profitieren die neuen Absorber von vergrößerten Prozessfenstern für eine optimale Leistung in Bezug auf den Ga-Gehalt, die Bandlücke und die reduzierten Abscheidungstemperaturen. Schnellere Abscheidungsraten werden in der kritischen 3. Stufe des Abscheidungsprozesses ermöglicht. Die anderen Abscheidungen, Prozesse und die Kontrollanalytik sind ähnlich effektiv wie bei CIGS, wobei Anpassungen mit leicht reduzierten erforderlichen Alkalimengen und überarbeiteten P1- und P3-Strukturierungsprozessen für monolithische Verbindungen vorgesehen sind. Das Verhalten bei Stresstests ist ausgezeichnet. Abgesehen von der Anpassung an die Modulstrukturierung sind die mit dem neuen Prozess identifizierten Herausforderungen spezifisch für das Labor und nicht relevant für die Herstellung. Das ACIGS-Projekt deutet daher auf eine zuverlässige Verbesserung der photovoltaischen Leistungen, erweiterte Prozesstoleranzen und eine vorläufig niedrige Barriere für die Anpassung bestehender CIGS-Prozesslinien hin.

Résumé

L'Empa a développé un procédé de fabrication de cellules et de modules solaires flexibles en Cu(In,Ga)Se2 (CIGS) sur des feuilles de polymère. Toutefois, la complexité du procédé et l'étroitesse des fenêtres de paramètres entraînent un écart entre l'efficacité des dispositifs en laboratoire et dans l'industrie. Le projet vise à résoudre ce problème en développant un nouveau procédé pour le CIGS sur film polymère qui sera plus simple, plus facile à contrôler et plus robuste tout en maintenant ou en améliorant les performances élevées démontrées précédemment.

L'approche d'alliage choisie a donné d'excellents résultats avec de minuscules quantités d'Ag d'environ 2 % par rapport au Cu (0,5 % au total). Nous avons démontré une cellule solaire CIGS certifiées sur des substrats flexibles en polyimide avec un rendement record de conversion d'énergie de 22,2 %. L'Ag peut être incorporé en tant que couche précurseur ou par différentes variantes de coévaporation avec une amélioration similaire de l'efficacité de 0,5-1%, ce qui laisse les deux options ouvertes pour une mise en œuvre industrielle. Par rapport aux compositions sans Ag, les nouveaux absorbeurs bénéficient de fenêtres de processus élargies pour des performances optimales en termes de teneur en Ga, de bande interdite et de températures de dépôt réduites. Des taux de dépôt plus rapides sont possibles lors de la 3e étape critique du processus de dépôt. Les autres dépôts, processus et analyses de contrôle sont aussi efficaces que pour le CIGS, des adaptations étant prévues avec des quantités d'alcali requises légèrement réduites et des processus de modelage P1 et P3 révisés pour les interconnexions monolithiques. Le comportement lors des tests de stress est excellent. Hormis l'adaptation au modelage des modules, les difficultés identifiées avec le nouveau procédé sont spécifiques au laboratoire et sans rapport avec la fabrication. Le projet ACIGS laisse donc entrevoir une amélioration fiable des performances photovoltaïques, un élargissement des tolérances du processus et une faible barrière pour l'adaptation de lignes de fabrication CIGS existantes.

Summary

Empa has developed a manufacturing process for flexible Cu(In,Ga)Se_2 (CIGS) solar cells and modules on polymer foils. However, process complexity and narrow parameter windows result in a gap between device efficiencies in the laboratory and industry. The project aims to address this issue by developing a new process for CIGS on polymer film that will be simpler, easier to control, and more robust while maintaining or improving the high performances previously demonstrated.

The chosen alloying approach has delivered excellent results with already tiny Ag amounts of about 2% versus Cu (0.5% overall). We demonstrated an externally certified record CIGS solar cell on flexible polyimide substrates with 22.2% power conversion efficiency. Ag can be incorporated as a precursor layer or by different variants of co-evaporation with similar 0.5-1% efficiency improvement, leaving both options open for industrial implementation. Compared to Ag-free compositions, the new absorbers benefit from enlarged process windows for optimal performance in terms of Ga content, bandgap, and reduced deposition temperatures. Faster deposition rates are enabled in the critical 3rd stage of the deposition process. The other depositions, processes, and control analytics are similarly effective as with CIGS, with adaptations foreseen with slightly reduced required alkali amounts and revised P1 and P3 patterning processes for monolithic interconnections. Behavior during stress tests is excellent. Apart from the adaptation to module patterning, the challenges identified with the new process are specific to the laboratory and irrelevant to manufacturing. The ACIGS project therefore points to a reliable improvement in the photovoltaic performances, widened process tolerances, and a tentatively low barrier for adaptation of existing CIGS processing lines.

Contents

Zusammenfassung **3**

Résumé **3**

Summary **4**

Contents **5**

Abbreviations **6**

1 Introduction **7**

1.1 Context and motivation 7

1.2 Project objectives 8

2 Procedure, method, results and discussion **10**

2.1 WP 1 Silver for high efficiency solar cells on polymer foils 11

2.1.1 Task 1.1 Optimal Ag incorporation method 11

2.1.2 Task 1.2 Absorber tailoring: bandgap and process optimization 15

2.1.3 Alkali treatments for interface tuning and absorber doping 18

2.2 WP 2 Industry-compatible processing 22

2.2.1 Task 2.1 Absorber deposition at low temperature 22

2.2.2 Task 2.2 Back contact formation 26

2.2.3 Task 2.3 Simple, fast and robust deposition processes 28

2.3 WP 3 Mini-modules and device stability 31

2.3.1 Task 3.1 Mini-module development by laser patterning for interconnections 31

2.3.2 Device performance stability 35

2.4 Related developments 37

2.4.1 Absolute photoluminescence tool 37

3 Conclusions and outlook **38**

4 Bibliography **42**

Abbreviations

List of used abbreviations:

AAC	[Ag]/([Ag]+[Cu]). Ag fraction amongst group-I Ag and Cu elements.
ACIGS	$(Ag,Cu)(In,Ga)Se_2$
CBD	Chemical bath deposition
CGI	[Cu]/([Ga]+[In]). Cu amount compared to group-III In and Ga elements.
CIGS	$Cu(In,Ga)Se_2$
CTM	Cell-to-module
EQE	External quantum efficiency
ERE	External radiative efficiency
GGI	[Ga]/([Ga]+[In]). Ga fraction amongst group-III In and Ga elements.
HLS	Heat-light soaking (treatment)
I/III	Ratio of group-I to group-III elements ([Ag]+[Cu])/([Ga]+[In]).
J_{SC}	Short-circuit current density
PDT	Post-deposition treatment
PI	Polyimide
PL	Photoluminescence
PLQY	Photoluminescence quantum yield
PV	Photovoltaic
SEM	Scanning electron microscopy
SLG	Soda-lime glass
TRPL	Time-resolved photoluminescence
V_{OC}	Open circuit voltage

1 Introduction

1.1 Context and motivation

The content of this section is reproduced from the proposal with modifications. The context timeline refers to the start of the project.

Empa has developed over the years a complete manufacturing process for flexible CIGS solar cells and mini-modules on flexible polymer foils. On the laboratory scale, the highest record solar cell efficiency demonstrated is 21.4% (certified measurement), but still significantly behind state-of-the-art of rigid CIGS technology (23.35% cell on glass) and of the market-dominant silicon. The flexible CIGS PV technology is particularly suitable for specific types of BIPV and mobility applications where lightweight and small volume footprint provides decisive advantages and allow premium prices.

The device power conversion efficiency is a crucial assessment point for a PV technology. Together with device performance stability, high power conversion efficiency ensures the long-term energy yield and ultimately decides the relevance of photovoltaic installations. The performance of flexible CIGS devices is limited by carrier recombination occurring in the CIGS absorber and at its front interface. Alloying of the CIGS matrix can improve a range of key material characteristics, resulting in recent performance boosts for absorbers processed at high temperatures on glass substrates. This alloying approach is especially appealing for low-temperature CIGS deposition processes on polymer foil as it precisely addresses some of the known process limitations.

Despite its successes and cell efficiency >21%, the CIGS process developed at Empa suffers from weaknesses when it comes to industrial adaptation. A first weakness is the process complexity of the CIGS absorber deposition - accumulated over years of development and optimization. The process suffer from poor robustness as parameter windows are relatively narrow for different parameters such as absorber composition including gradients, substrate temperature or details of the alkali treatments. Highest record efficiencies are achieved but with a significant dispersion in cell, and the complex deposition process requires strict parameter control and multiple sequential steps. Such requirements are very challenging to materialize in an industrial production environment. As consequences, the process transfer from lab to fab is not straightforward and the gap in device performances between laboratory and industry is larger than desired.

The efficiencies of industrially-produced monolithically connected large area flexible solar modules on polymer film are in the range of 10%-12.5%, while solar cells are about 15% efficiency. Clearly, this low efficiency severely restricts the applicability of modules to limited niche markets. While scientific insights and technical progresses made during last years indicate the prospects for higher efficiency of industrial modules, some modifications to the process and equipment will be essential – first to prove in the laboratory, then later on up-scale in stepwise manner.

1.2 Project objectives

The content of this section is reproduced from the proposal with minor modifications.

Therefore, while until now Empa focused on improving record device efficiencies, the project is planned to solve those problems by developing a significantly lower temperature process for CIGS on polymer film that will be simpler, easier to control and more robust, while maintaining or even improving the high performances demonstrated by existing processes. The process should reduce the mechanical stress, enable reduced deposition temperatures by as low as 100°C and eventually allow higher growth rate.

The project targets 4 main objectives:

- A simplified fabrication process for high efficiency flexible CIGS devices on polymer with relaxed manufacturing tolerances intended for reduced lab-to-fab performance gap. Low sensitivity (device performance loss < 1%) to process simplifications or to variations in parameters:
    - Reduced number of steps (corresponding to number of sources in an inline process)
    - Supply of alkali element reduced two-fold – conversely, sped up alkali deposition steps
    - Deposition temperature reduced by 100°C
    - Modified absorber composition (bandgap variations between 1.1 and 1.2 eV, 5% variation on group-I/group-III composition ratio)
- New process transferability to industrial production:
    - Detailed comparison of methods for absorber alloying to identify which option is most suitable in view of roll-to-roll production (precursor or coevaporation)
    - Quantified kinetic limits of new process in view of faster deposition
    - Low-losses interconnections for module making (<3% cell-to-module losses yielding 20% efficiency)
    - Stable device performance at cell and module levels under stress test conditions
- Formalize a blueprint roadmap for industrial process scale-up and lab-to-fab technology transfer
- Demonstrate technology potential: cell efficiency improved to 23% on flexible foils.

Anticipated results

We will demonstrate a simpler, more robust deposition process and boost the device efficiency, for both laboratory and industrial types of processing. The new process will feature higher deposition speed, improved throughput and lower thermal budget for savings in energy and time for heating and cool-down. We anticipate an easier scale-up of laboratory findings to industry, helping to bridge the device efficiency gap from lab to fab.

The implementation of our findings in an industrial environment would require modifications to one or several processing equipment. However, at this early stage the specifics of what type of modifications in industrial roll-to-roll manufacturing equipment and processes are not adequately clear. In order to provide a clear and convincing case to the industry, we need to address the following aspects, formalized into a blueprint roadmap for industrial manufacturing.

- Identify the optimal incorporation method of Ag and alkali incorporation procedures
- Quantify the expected benefits at the laboratory scale (performance, process tolerances etc.)
- Clarify the required adaptions to current processes

- Prove the transfer-ability of the findings to the industrial environment and identify what type of modifications will be required in roll-to-roll industrial machines.

We will also investigate aspects more directly related to material science that may offer positive side-effects on manufacturing:

- The stress in the absorber layer is relaxed, with positive impacts in reduced cracking, delamination and in module patterning.
- Impact of modified absorbers and processes on the formation of the back contact and inter-connections, in terms of material properties, performances and processability.
- Optimal strategies for absorber doping and alkali incorporation. Reports indicate that a lesser amount of alkali metals is required for ACIGS as compared to CIGS, which is favourable in view of high throughput processing. The fundamental reasons behind this observation, the interplay with grain size, the impact on the alkali incorporation strategy, and new process tolerances must be clarified.
- Improvements in the understanding and control of the CIGS material and devices processed with high growth rate.

2 Procedure, method, results and discussion

To address the research questions and to maximize the impact of the project, the project organizes the activities in three Work Packages. The report is structured accordingly:

1. WP1 Silver for high efficiency solar cells on polymer foils
   Device efficiency is a key factor for PV applications. At lab scale, it signifies the potential of the technology, influences perception of interested parties and provides directions for future technology transfers. At large scale the device efficiency determines the electricity generation and ultimately the profitability of PV installations. We identify the best method to realize the absorber alloying, to determine the process sequence and clarify which deposition equipment must be used or modified. We investigate the required process modifications induced by absorber alloying, on absorber composition (group-I and group-III composition ratios, gradients), and possible comparative advantages related to alkali elements. Slow, well-controlled processes are used to facilitate investigation. We explore and develop these methods, to improve device performances and establish clear guidelines for technology transfer. These questions are addressed in WP1.
2. WP2 Industry-compatible processing
   Industry-compatible processing is crucial to provide best chances for successful technology transfer and reduce the lab-to-fab device efficiency gap. In this context, we divert from process optima and investigate the processing limits and tolerances regarding the following aspects: lower substrate temperatures, impact on formation of back contact and substrate adhesion, simplified process (esp. number of steps that corresponds to a number of individual sources in an inline process). Our goal is to facilitate industrial implementation, enhance process robustness, increase possible deposition speeds, and address the issues relevant from an industrial processing point of view. These very important topics are detailed and addressed in WP2.
3. WP3 Mini-modules and device stability
   Validation of the new processes in view of industrialization, by adapting the process for monolithic interconnections for mini-modules to the new absorbers, and assessment of the device stability under stress conditions. The validation is performed within WP3.
4. Related developments are also reported, no foreseen during project planning but that proved invaluable to the project success.

2.1 WP 1 Silver for high efficiency solar cells on polymer foils

2.1.1 Task 1.1 Optimal Ag incorporation method

Description of experiments

To perform the work, a new evaporation source (effusion cell) was ordered and was installed into the CIGS evaporation reactor in 2022.

We investigated two different methods for Ag incorporation and compare them, aiming to provide a decision basis in view of the industrialization of the new deposition process. Absorber layers were prepared by modified 3-stage processes with advanced alkaline treatment, using flexible Mo-coated polyimide (PI) foils as substrates. Ag was incorporated according to the methods shown in Figure 1: by precursor layer ex-situ method or by in-situ co-evaporation of Ag metal during the CIGS deposition. For both approaches, the amount of Ag was kept small as compared to Cu (<10% AAC [Ag]/([Ag]+[Cu])).

- For the precursor method, 10, 15, and 20 nm thick Ag metal layers were deposited on the substrates in a separate chamber. CIGS layers were deposited on top of the precursor layer.
- For the co-evaporation approach, elemental Ag was co-deposited at the beginning (Method 2), together with Cu during the 2nd stage (Method 3), and during the 3rd stage of the absorber deposition process (Method 4), as shown in Figure 1.

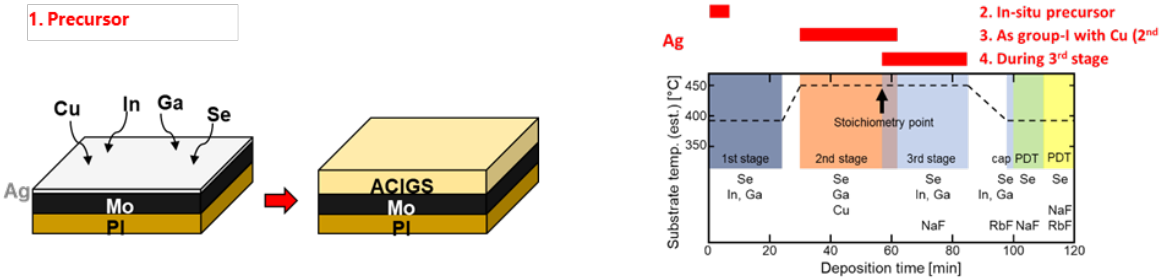

Figure 1: Graphical representation of the ACIGS preparation process. (left) (1) For the precursor method, we evaporate a metal Ag layer before the CIGS deposition process. (right) For the co-evaporation method, the CIGS 3-stage process with advanced alkali treatment was modified with (2) an additional Ag evaporation step at the beginning, (3) with Cu in 2nd stage, and (4) during 3rd stage in the deposition process.

Comparison of Ag incorporation methods

The microstructure of the resulting ACIGS layers is shown in Figure 2. It is clearly shown that incorporating Ag favors more extensive grain growth as compared to the reference CIGS layer. Only with Method 4 (Ag co-evaporation during the 3rd stage) does the absorber morphology appear improved, but only in the upper part of the absorber. With this method, Ag is incorporated only after the Cu-chalcopyrite phase is formed throughout the entire thickness of the absorber film. The Cu-Ag interdiffusion is presumably too slow to allow further recrystallization and grain growth of the film, down to the back contact.

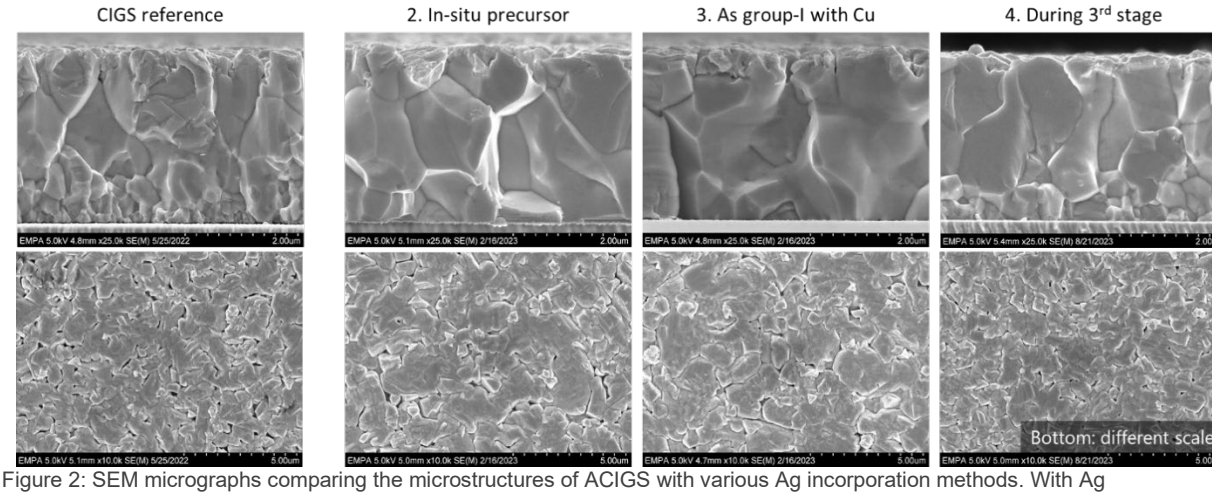

Figure 2: SEM micrographs comparing the microstructures of ACIGS with various Ag incorporation methods. With Ag incorporation, grains effectively grow larger than for reference CIGS absorbers.

The photovoltaic performances of the corresponding devices are listed in Table 1. The efficiency values reported are without anti-reflective coating. All Ag incorporation methods achieved excellent solar cell performance approaching or exceeding 21%. The alloying with Ag benefits the layers and solar cell devices in a very similar manner, independently from the incorporation method.

Table 1: Sample details and photovoltaic performances of ACIGS solar cells obtained by the investigated Ag incorporation methods. The composition ratio ACGI stands for ([Ag]+[Cu])/([Ga]+[In]), and GGI for [Ga]/([Ga]+[In]).

Run		Ag introduction	T sub	AAC	ACGI	GGI	Best Cell				Average			
			Max				eff. %	V_{OC} mV	J_{SC} mA/cm^2	FF %	eff. %	V_{OC} mV	J_{SC} mA/cm^2	FF %
2101	CIGS	w/o	450 (350)	-	0.96	0.40	20.6	742	36.3	76.5	20.4	736	36.5	75.9
2106	Pre-ACIGS	(1) Precursor	450 (350)	0.02	0.97	0.40	20.6	754	36.1	74.8	20.4	758	36.1	74.4
2095	ACIGS	(2) Co 1st beginning	450 (350)	0.03	0.99	0.40	21.2	760	36.1	77	20.7	754	35.9	76.6
2242	ACIGS	(2) Co 1st beginning	450 (350)	0.03	0.96	0.39	21.3	753	37.0	76.6	20.9	753	36.3	76.6
2247	ACIGS	(2) Co 1st beginning	450 (350)	0.02	0.94	0.40	21.3	763	36.1	77.1	20.9	760	36.0	76.6
2256	ACIGS	(2) Co 1st beginning	450 (350)	0.02	0.95	0.39	21.2	757	36.4	77.1	21.0	755	36.2	77.0
2259	ACIGS	(2) Co 1st beginning	450 (350)	0.02	0.96	0.39	21.1	764	36.0	76.9	20.8	758	35.8	76.8
2263	ACIGS	(2) Co 1st beginning	450 (350)	0.03	0.95	0.39	21.3	767	35.7	77.7	21.1	761	35.9	77.1
2267	ACIGS	(2) Co 1st beginning	450 (350)	0.02	0.96	0.38	21.4	763	36.5	76.8	21.0	759	36.3	76.4
2317	ACIGS	(2) Co 1st beginning	450 (350)	0.03	0.97	0.41	21.0	766	36.4	75.2	20.7	767	35.8	75.6
2323	ACIGS	(2) Co 1st beginning	450 (350)	0.03	0.96	0.40	21.2	765	36.1	76.9	21.1	764	36.0	76.8
2241	ACIGS	(3) Co 2nd with Cu	450 (350)	0.02	0.95	0.40	21.2	746	37.1	76.6	20.9	747	36.5	76.6
2257	ACIGS	(3) Co 2nd with Cu	450 (350)	0.02	0.95	0.38	21.3	765	35.9	77.7	20.9	760	35.8	77.0
2258	ACIGS	(3) Co 2nd with Cu	450 (350)	0.02	0.96	0.39	21.2	765	35.9	77.1	20.8	757	35.9	76.6
2316	ACIGS	(3) Co 2nd with Cu	450 (350)	0.02	0.98	0.42	20.9	771	35.5	76.5	20.6	764	35.5	76.0
2319	ACIGS	(4) Co 3rd with In+Ga	450 (350)	0.02	0.96	0.40	21.3	760	36.1	77.4	21.0	757	35.9	77.4
2326	ACIGS	(4) Co 3rd with In+Ga	450 (350)	0.01	0.94	0.39	21.3	751	36.7	77.4	20.7	743	36.1	77.2
2334	ACIGS	(4) Co 3rd with In+Ga	450 (350)	0.02	0.96	0.38	21.2	756	36.7	76.4	21.0	754	36.5	76.5
2348	ACIGS	Co in cap	450 (350)	0.02	0.95	0.38	20.2	728	37.2	74.7	19.9	727	36.5	74.9
2349	ACIGS	Co end of 3rd	450 (350)	0.02	0.96	0.37	20.5	724	37.0	76.5	20.3	722	36.8	76.4

To confirm the limits for Ag incorporation, we tested extreme situations believed to be inappropriate. One is Ag co-evaporation for only a short time (2 min) at the end of the 3rd stage, and the other is during cap deposition only. The intention is to observe the later limits for the Ag diffusion in the layer and the improvement in device performance. The results are also listed in Table 1. As expected, both samples show no apparent improvement in V_{OC}, yet at the same time, they perform similarly well as

the reference CIGS cell. The results suggest that incorporating low 2% Ag versus Cu amounts into a CIGS layer is almost no risk for the device performance compared to the reference CIGS preparation method. Improved efficiencies are obtained when Ag is available before the 2nd stoichiometry point at the latest, irrespective of the incorporation method (see Figure 3).

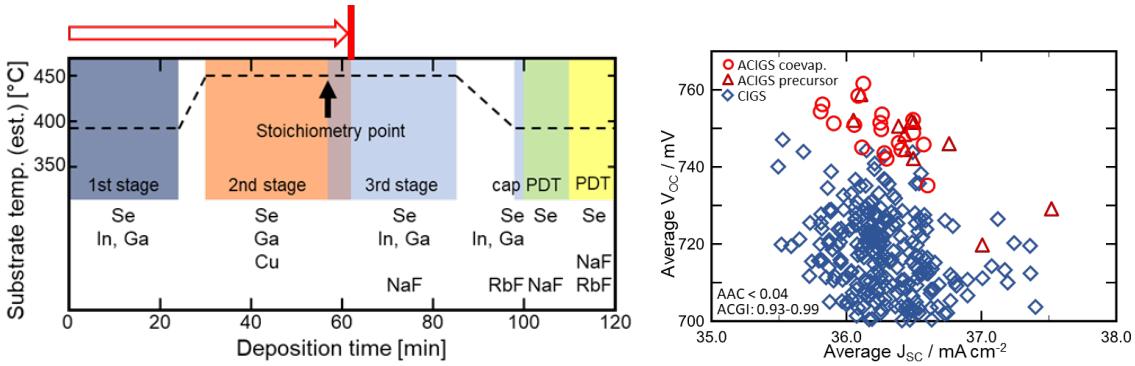

Figure 3: (left) Improvement in photovoltaic performance is obtained when Ag is provided to the absorber, the latest before the 2nd stoichiometry point, irrespective of the tested incorporation method. (right) J_{SC} vs V_{OC} of CIGS and ACIGS solar cells. The values displayed are average cell performance of individual samples (up to 18 solar cells on a sample). The dataset is restricted to absorber compositions ratios AAC < 0.04 and 0.93 < ACGI (I/III) < 0.99. Ag alloying has a clear positive impact on V_{OC}.

Impact of silver on PV parameters

To acquire statistical confidence, we compared V_{OC} and short-circuit current (J_{SC}) for CIGS and ACIGS solar cells. As visible in Figure 3(right), Ag alloying improves V_{OC} by 15-20 mV for a given J_{SC}. Little change is observed regarding FF. On the other hand, we observe no striking difference between coevaporation and precursor processes. We conclude that the main improvement by Ag incorporation is V_{OC}.

To better understand the changes brought by Ag alloying and the reason for the V_{OC} increase, we acquired further analytics was acquired on a series of samples with similar composition and gradient. Figure 4 shows the effect of Ag incorporation on the apparent doping density. For the conditions corresponding to our record cells (low Ag content AAC~2%), we attribute the V_{OC} increase to the higher doping concentration as shown in Figure 4(left), which is partly counterbalanced by a slight reduction in TRPL carrier lifetimes from 350 down to about 200 ns (not shown). On the other hand, samples with higher Ag concentration (AAC about 5%) do rather seem to present a reduction in doping density upon Ag incorporation. These results are not necessarily in contradiction. ACIGS absorbers with considerably higher Ag content (e.g. 20% AAC) are known to feature a very low doping level. Moreover, treatment with alkali elements may play an important role in the changes in doping density, and it is possible that the treatments applied were not optimal as discussed in the following Sections.

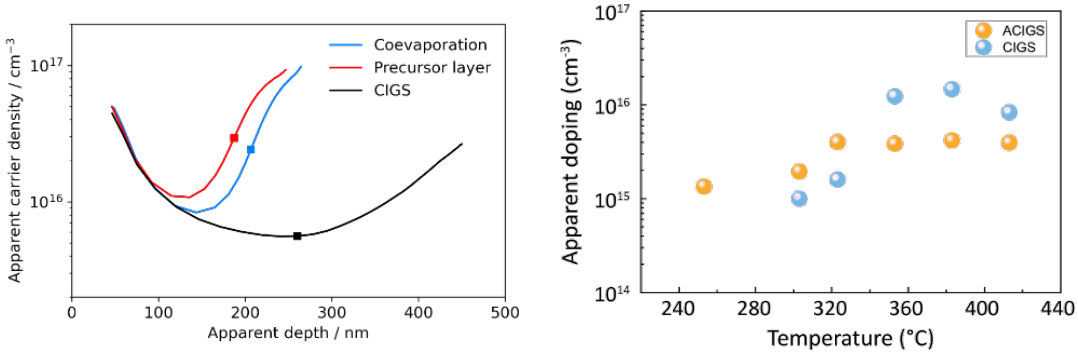

Figure 4: Change in apparent carrier density for Ag-alloyed ACIGS solar cells. (Left) Apparent doping concentration as function of apparent absorber depth (absorbers with AAC: ~2%). (Right) Apparent doping density for ACIGS solar cells with reduced nominal deposition temperature (AAC: 4-5%).

Record ACIGS solar cells

Record CIGS cells on flexible PI substrates were obtained with efficiency above 22%, externally certified values as shown in Figure 5. Such results were obtained with both co-evaporation and precursor layer approaches Compared to the previous best mark, the performance increase is driven by open-circuit voltage. A statistical analysis was also conducted, demonstrating that Ag alloying improves V_{OC} by 15-20 mV for a given J_{SC}. Little change was observed regarding FF. We concluded that the main improvement by Ag incorporation is V_{OC}.

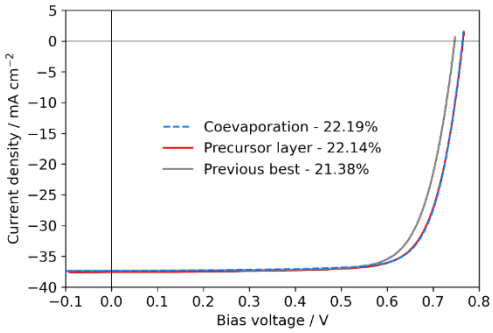

Figure 5: Certified efficiency of ACIGS and previous CIGS record solar cells on flexible PI substrates. Devices with record efficiencies >22% were obtained with both coevaporation and precursor methods.

2.1.2 Task 1.2 Absorber tailoring: bandgap and process optimization

In this task, we evaluate the impact of absorber composition and required compositional gradients in terms of Ag amount quantified by the ratio AAC ([Ag]/([Ag]+[Cu])) and Ga amount GGI ([Ga]/([Ga]+[In])).

Optimal amount of silver

The effects of Ag amount (AAC) and of Ga amount (GGI) were evaluated. Figure 6(left) shows the effect of Ag content AAC on the solar cell efficiencies. Data corresponding to CIGS absorbers are also shown in black for comparison. The best device performance is observed with AAC of about 2% as compared to Cu. For low Ag concentrations AAC < 4%, the V_{OC} increases by about 15-20 mV. The reason for the decrease in efficiency with higher AAC values >4% is not clear. It is known that excellent devices can be made with AAC ratios of 20% or more. We speculate that the use of higher Ag concentrations requires more thorough revision of the absorber deposition process notably regarding the specifics (amount, duration, time) of alkali Na and Rb treatments.

Figure 6(right) shows the impact of GGI on the V_{OC}. The Ga content GGI has a strong impact on the compositional gradient formation and on the absorber bandgap: a higher GGI leads to higher bandgap, which should result in higher V_{OC} values.

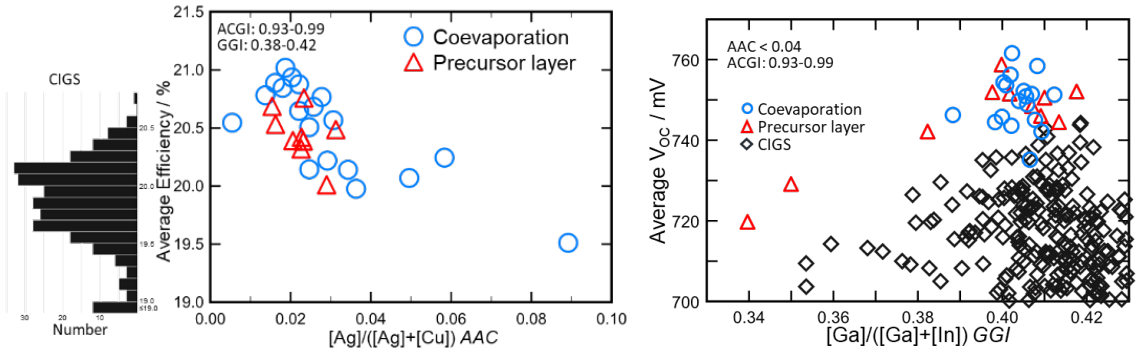

Figure 6: (left) Solar cell efficiency as function of the Ag content AAC. The device efficiencies are maximum around AAC~2%. As compared to the CIGS (left histogram), Ag alloying leads to an increase in efficiency by about 0.5%. (right) Average V_{OC} depending of GGI. A 15-20 mV V_{OC} increase is observed for a given GGI.

Impact of absorber composition and bandgap

Figure 7 shows the additional statistics of solar cell photovoltaic parameters as functions of the Ga content GGI. The ACIGS data series is restricted to absorbers with AACs ratios of about 2%. The incorporation of Ag increases the open-circuit voltage V_{OC} by 10-20 mV and increases the power conversion efficiency by about 0.5-1.0 % absolute, over the whole tested GGI composition range.

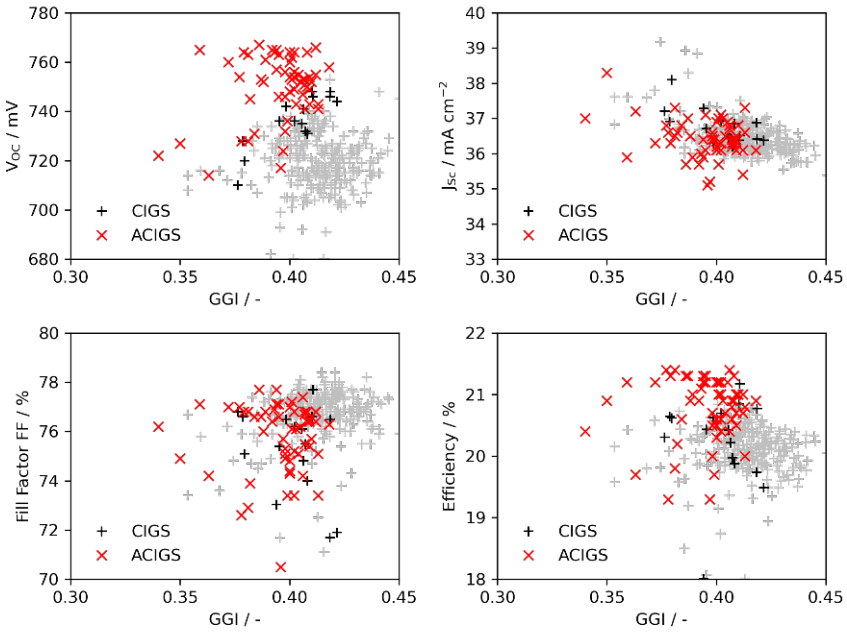

Figure 7: Statistics of solar cell efficiency as functions of the Ga content GGI, which can be used as a proxy for the absorber bandgap energy. The ACIGS dataset is restricted to absorbers with AAC ratios of about 2%.

Figure 8 shows external quantum efficiency (EQE) curves of selected cells with various optical bandgaps. The bandgap-dependent photovoltaic parameters of this specific set of solar cells are reported in Figure 9. To underline the significance of the values, the Shockley-Queisser limit is also indicated together with a few derived variations. In addition, the cells' external radiative efficiency (ERE) extracted from EQE and V_{OC} i, which relate to non-radiative recombination loss, is also shown.

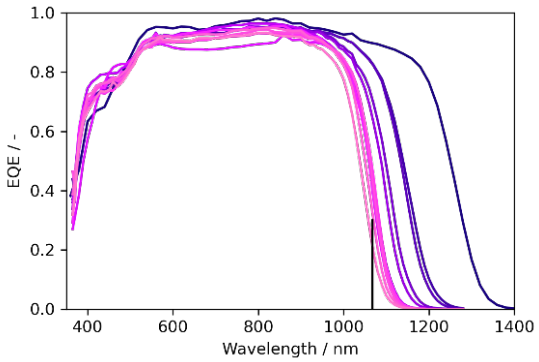

Figure 8: External quantum efficiency curves of selected cells with different bandgaps. The corresponding PV performances are reported in Figure 9. For quick estimation purposes, the bandgap energy can be estimated at the energy for which the EQE value is about 25%.

The photovoltaic performance is then investigated as function of the optical bandgap extracted from EQE, as shown in Figure 9. The optimum power conversion efficiency is obtained over a wide range of bandgap energy values, from 1.12 to 1.16. This optimum composition appears wider than with regular CIGS. Below 1.16 eV absorber bandgap energy, the performance follows the trend imposed by the Shockley–Queisser limit. Additionally, we observe a slight reduction in FF at the lowest investigated bandgaps. Above 1.16 eV bandgap, a fast degradation in FF is observed, and the V_{OC} starts to saturate, with a corresponding degradation in ERE values. The degradation of device performance with bandgap >1.16 eV is commonly observed for CIGS. One hypothesis is the presence of defects entering within the bandgap when the Ga content is high enough to ensure Eg ≥ 1.35 eV [ii]. While not

active within the bandgap minimum region of the compositional graded absorber, the reduced energy difference to the bandgap minimum may induce a larger residual population of minority carriers and therefore increase non-radiative recombination. In this hypothesis, possible paths forward could be to properly address the presence of the detrimental defects, or lower the bandgap of the absorbers.

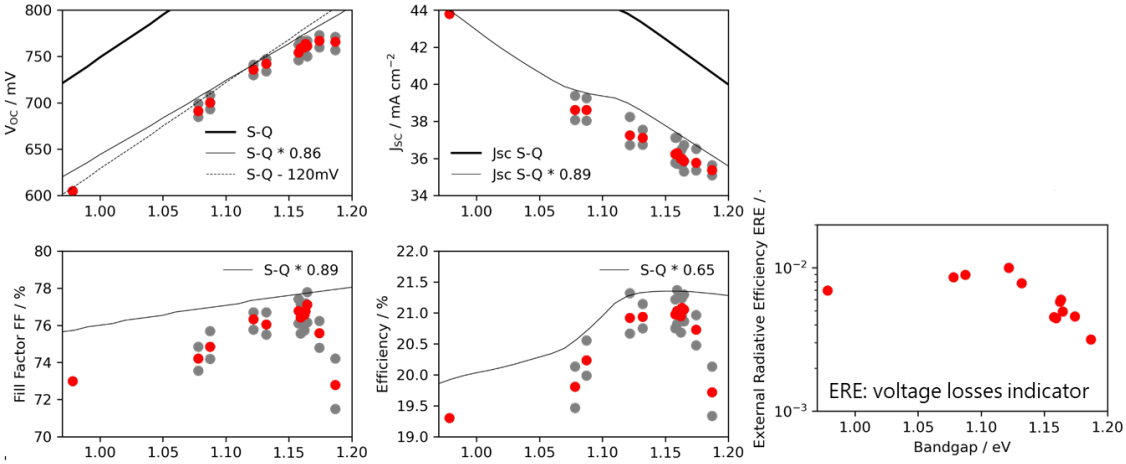

Figure 9: PV performances against bandgap of ACIGS cells (top four figures). Red points indicate the average and grey points correspond to the best and worst cell from each process run. The external radiative efficiency (ERE) calculated from EQE curves and V_{OC} values is also reported, which indicates the impact of non-radiative recombination losses.

2.1.3 Alkali treatments for interface tuning and absorber doping

Initial hints from private communication with other laboratories and literature, suggests that a reduced amount of alkali is required for Ag-alloyed absorbers. This reduction is tentatively due to the improved morphology with reduced density of grain boundaries, and in relation to the facilitated Ga-In interdiffusion. While variations in process specifics can easily be modified in the laboratory, clear indications are required in view of upscaling where the equipment design limits the process freedom.

Optimal NaF and RbF amount

Initial experiments focused on the amount of both NaF and RbF incorporated during the PDT process, achieved by varying the temperature of the evaporation sources.

We observed little to no difference with sodium, brought in the layers by means of a NaF post-deposition treatment PDT. Excessive amounts do not appear as an issue to device performances, and the excess is washed away during rinsing of subsequent wet deposition of the buffer layer by chemical bath deposition (CBD).

The heavy alkali rubidium is also brought in by PDT method. The optimum treatment is rather similar for CIGS and ACIGS layers. Possibly, the optimum in RbF source temperature might be reduced for ACIGS compared to CIGS by 5°C. To place the number in context, this is a minor change as the amount of evaporated material is reduced by about 15%. Yet, the optimum in source temperature is at least as wide as this change in optimum setting, as this one can only be provided with a confidence of ±10°C, as can be seen in Figure 10.

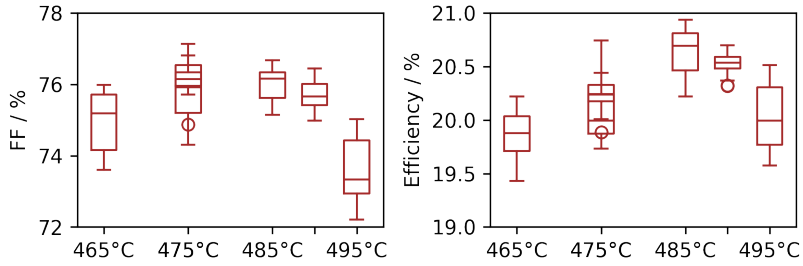

Figure 10: FF and efficiency of ACIGS solar cells with different temperatures of the RbF evaporation source during PDT. An optimum is identified, driven by a lower FF on the high side, and a combination of the PV parameters factors on the low side.

Process simplification, acceleration, and reduction of heavy alkali amount

Simplification of PDT and reduction of the amount and process times for alkali elements were investigated, as illustrated in Figure 11. The process is simplified by removing one temperature step during PDT keeping temperature constant 290°C, and decreasing the PDT process duration from 40 min to 20 min. The modified process was first developed using CIGS absorbers and then extended to Ag-alloyed ACIGS absorbers.

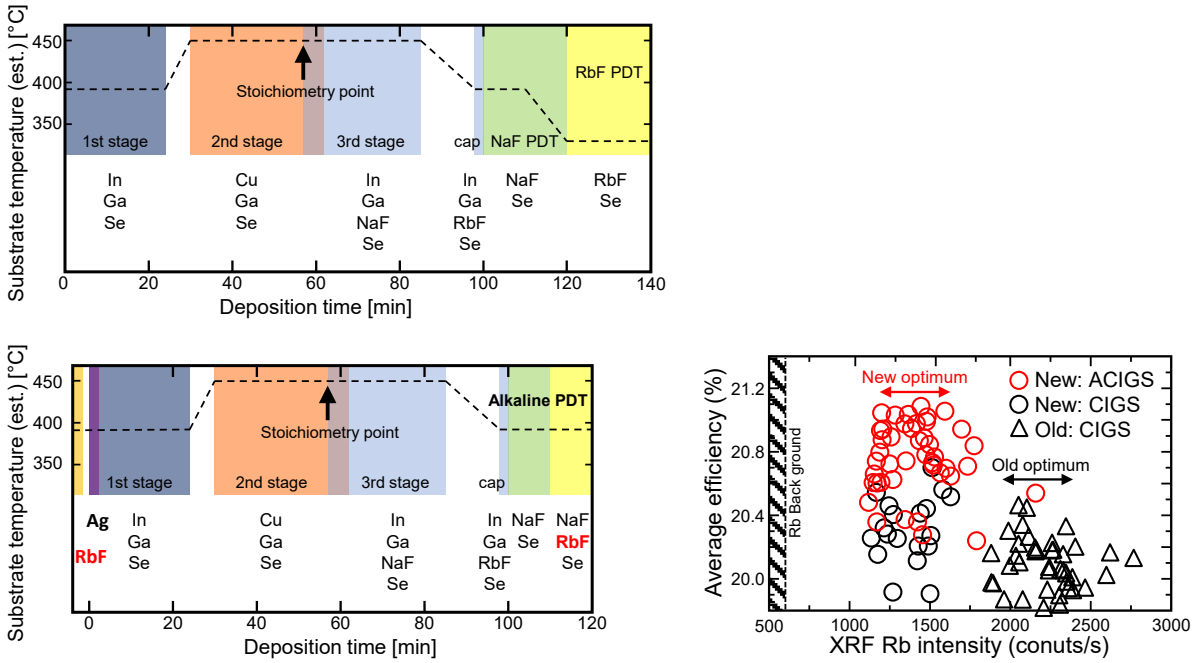

Figure 11: (top) Graphical representation of the old CIGS standard process (bottom) Graphical representation of the newly developed ACIGS preparation process. Rb was incorporated only by PDT, or by RbF precursor and PDT. (right) Effect of Rb amount on the efficiency for ACIGS and CIGS samples prepared using new and old processes

Figure 11(right) presents the effect of Rb amount on the efficiency (average of cells on one substrate). The modified, shorter process leads to a slight improvement in the efficiency of CIGS cells, and a larger improvement in ACIGS devices. As compared to CIGS, ACIGS by modified process shows excellent reproducibility and a gain about 0.5 point % of efficiency. As a result of the modification and optimization of the PDT, the Rb amount in absorber was reduced from 2.0-2.4x10^3 to 1.2-1.6x10^3 counts/s in XRF intensity for the optimum condition. Considering the background intensity of Rb (about 0.6x10^3 counts/s), the optimum Rb amount for modified process is about half that of the old process. Owing to the improved performance, the modified process was adopted as the baseline process.

Figure 12(left) shows the Rb and Na depth profiles in high efficiency CIGS and ACIGS devices, obtained by SIMS. As compared to CIGS, the ACIGS absorber present a clear decrease in both elements in the bottom half of the layers. This can be attributed to the difference of grain size at the bottom of layers (see deliverable D1.1 Figure 2). Near both top and bottom interfaces, a similar signal can be observed in both optimized CIGS and ACIGS absorbers.

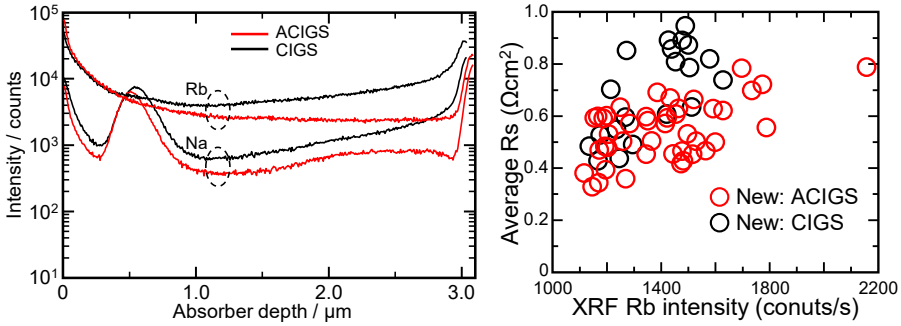

Figure 12: (left) The depth profiles of Rb and Na in ACIGS and CIGS layers analyzed by SIIMS. (right) The effect of Rb amount on the series resistance of ACIGS and CIGS cells. Rb was only incorporated by PDT.

Figure 12(right) shows the effect of the Rb amount on the series resistance. As stated above, the best device efficiencies are obtained with XRF Rb signal intensity in the range of 1.2-1.6x10^3 counts/s, for both of ACIGS and CIGS layers. On the other hand, the series resistance of ACIGS seems to increase slower with increasing Rb amount than CIGS. It must be mentioned that in our experiments, ACIGS devices did not show clear blocking behavior in JV curves measured at room temperature typical of CIGS absorber composition. We conclude that ACIGS absorbers are more robust to excessive Rb amounts than CIGS.

RbF as precursor layer

The ACIGS absorber deposition was modified with the introduction of a RbF precursor layer prior to the deposition. Presence of heavy alkali during the deposition affects the absorber synthesis. The approach proved very effective with low bandgap CIS absorber layers deposited at higher temperatures on glass substrates [iii]. ACIGS solar cells with RbF precursor layers reproducibly reach comparable efficiencies with those without RbF precursor.

To clarify the detail of the effect of RbF precursor, a well-controlled set of samples was chosen for detailed investigation. The thickness of the RbF precursor layer is controlled by the source temperature, a difference in 25°C source temperature leading to a factor of about 2. We note that the XRF signal intensities also measure Rb introduced later in the deposition process e.g. during the PDT process. Figure 13 shows the microstructure of ACIGS layers with RbF precursor. A layer composed of smaller grains is found at the bottom of the absorber, caused by the alkali precursor, and which thickness increases with Rb amount. Although the small grains at the bottom doesn't directory degrades PV performances especially when confined to the high bandgap region to the rear of the compositionally graded absorber, it demonstrates that RbF precursor does affect the grain growth and then its optoelectronic quality.

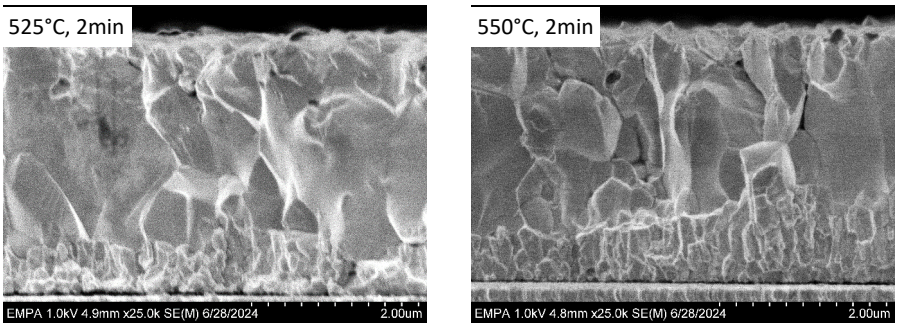

Figure 13: SEM cross section images of samples with RbF precursor. Left: Oct2466 (525°C,2min), Right: Oct2467 (550°C,2min)

Figure 14 presents a comparison of the efficiency and its distribution by box plot with RbF precursor. On the one hand, a clear efficiency drop is observed with the thickest RbF precursor layer (Figure 14 left), which is cause by a reduced Voc. On the other hand, all devices feature quite similar EQE responses (Figure 14 right), including the subbandgap tail states. Since all the ACGS layers have similar depth-integrated chemical composition, it is concluded that these solar cells have a similar shape of the band gap grading irrespective of the precursor layer and changes in the grain morphology.

Capacitance voltage as well as PLQY measurements were conducted to understand the voltage losses. A clear decrease in carrier density was observed with increasing RbF precursor thickness. In addition, the change in ΔV_{plqy} reasonably reflects the V_{OC} in devices. The voltage decrease somewhat exceeds what is expected from the decrease in doping level alone (20 mV), suggesting a simultaneous degradation in the electronic quality in terms of minority carrier lifetime. The PLQY provides good estimation of V_{OC} for high quality ACIGS devices.

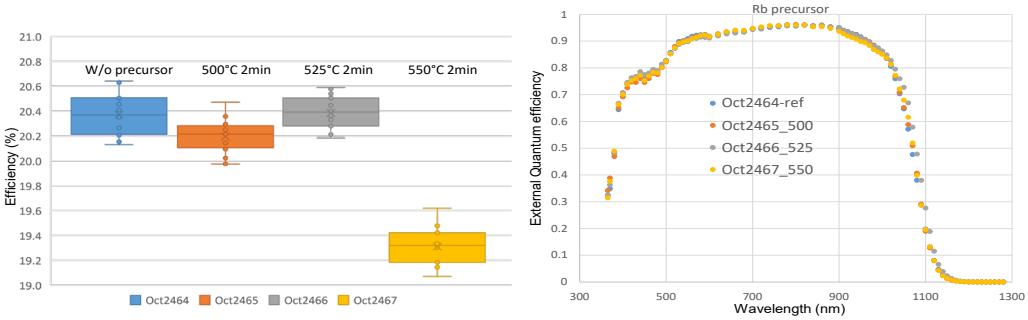

Figure 14: Comparison of PV properties of ACIGS solar cells prepared with RbF precursor layers with different thicknesses. (left) Box plot of solar cell efficiencies. (right) External quantum efficiency curves.

2.2 WP 2 Industry-compatible processing

2.2.1 Task 2.1 Absorber deposition at low temperature

Control of actual temperatures in large vacuum coater can be challenging for a variety of reasons (intense radiative heating from heated sources, presence of absence of heat sinks in roll-to-roll coating, metrology, optical or mechanical access to the area of interest, design flaws, etc.). It is therefore crucial to understand the impact of deviations in process temperatures, significantly below the upper limit imposed by the flexible polymer substrate.

PV properties

CIGS and Ag-alloyed CIGS absorbers were deposited at different deposition temperatures: standard, and reduced by 50°C or 60°C nominal. Table 2 reports the deposition temperatures and the resulting device photovoltaic parameters.

We note that the temperature measurement is challenging in vacuum. Therefore, we provide both nominal and (best guess) actual values. The nominal process temperature of 350°C is our standard for processing on flexible polyimide foils. The corresponding actual value is about 450°C. In this study, the temperatures were reduced by 50°C or 60°C nominal, yielding the estimates of the actual values 400°C and 390°C reported in Table 2. The actual temperatures are presumably even slightly lower, as the thermocouple temperature indication is correct at room temperature. The reduction in investigated temperature is more likely about 65°C and 75°C.

Table 2: Photovoltaic properties of selected solar cells with CIGS and ACIGS absorbers, comparing standard and reduced deposition temperatures. The temperature values reported are actual (nominal), such that the 450°C actual substrate temperature is the upper limit for processing on flexible polyimide foils. Each sample comprises up to 18 cells.

Run		Ag introduction	T sub max (°C)	AAC	ACGI	GGI	Best Cell				Average			
							Eff %	Voc mV	Jsc mA/cm2	FF %	Eff %	Voc mV	Jsc mA/cm2	FF %
2101	CIGS	w/o	450 (350)	-	0.96	0.40	**20.6**	742	36.3	76.5	20.4	736	36.5	75.9
2095	ACIGS	Co 1st beginning	450 (350)	0.03	0.98	0.40	**21.2**	760	36.1	77.0	20.7	754	35.9	76.6
2247	ACIGS	Co 1st beginning	450 (350)	0.02	0.94	0.40	**21.3**	763	36.1	77.1	20.9	760	36.0	76.6
2256	ACIGS	Co 1st beginning	450 (350)	0.02	0.95	0.39	**21.2**	757	36.4	77.1	21.0	755	36.2	77.0
2259	ACIGS	Co 1st beginning	450 (350)	0.02	0.96	0.39	**21.1**	764	36.0	76.9	20.8	758	35.8	76.8
	Low Temp.													
2255	CIGS	w/o	**390 (290)**	-	0.96	0.39	**18.0**	661	37.3	73.0	17.7	663	36.4	73.3
2255	CIGS on SLG						**18.7**	692	36.5	73.9	18.4	683	36.4	74.1
2254	ACIGS	Co 1st beginning	**400 (300)**	0.02	0.97	0.40	**20.9**	743	37.0	76.1	**20.7**	744	36.4	76.6
2248	ACIGS	Co 1st beginning	**390 (290)**	0.02	0.95	0.38	**20.6**	731	36.8	76.6	**20.3**	730	36.3	76.4

At standard temperature (450°C actual), the Ag-alloyed absorbers outperform the CIGS ones (>21% versus <21%), thanks to an improvement in open-circuit voltage V_{OC}.

Reducing the deposition temperature by about 60°C reduced the power conversion efficiency of the CIGS devices by about 2% absolute, primarily due to a substantial reduction in V_{OC} by about 50 mV and marginally due to a decrease in fill factor. This degradation follows a similar pattern in our previous investigation using SLG substrates. The V_{OC} degradation upon temperature reduction may appear slightly sooner with PI substrates than with rigid SLG ones.

Ag-alloyed absorbers show a much-improved resilience to reduced temperatures. For a similar near-stoichiometric absorber composition, the decrease in device efficiency is only about 0.5% absolute upon a 60°C temperature decrease. A 20.6% efficiency cell was demonstrated using this low deposition temperature. The decrease is also driven here by V_{OC}, yet it is considerably less than the Ag-free CIGS counterpart processed at the same temperature.

While reducing the deposition temperature by 60°C nominal leads to a measurable decrease in device performance, a slightly lesser reduction by 50°C resulted in an almost negligible device efficiency loss compared to reference devices obtained at the standard temperature.

We conclude that Ag alloyed drastically increases the process tolerance to low temperatures. The deposition temperature can be reduced by about 50°C with almost indistinguishable loss in device performance. A slightly more significant reduction in deposition temperature of 60°C results in a decrease in efficiency by about 0.5% absolute, while Ag-free CIGS counterparts already lose about 2%.

Absorber morphology

Figure 15 presents cross-section and top-view SEM micrographs of CIGS and Ag-alloyed ACIGS absorbers deposited at standard and reduced temperatures (-60°C nominal). As previously observed, Ag improves the morphology with larger grains throughout the depth compared to regular CIGS composition.

Reducing the temperature by 60°C dramatically impacts CIGS absorbers, with grain size markedly decreasing and a sharp increase in the number of holes and crevices visible on the cross-section images near the top of the absorber. By contrast, Ag leads to an absorber morphology similar to that of CIGS layers grown at 60°C higher temperatures, possibly slightly worse in the non-recrystallized top part of the absorber.

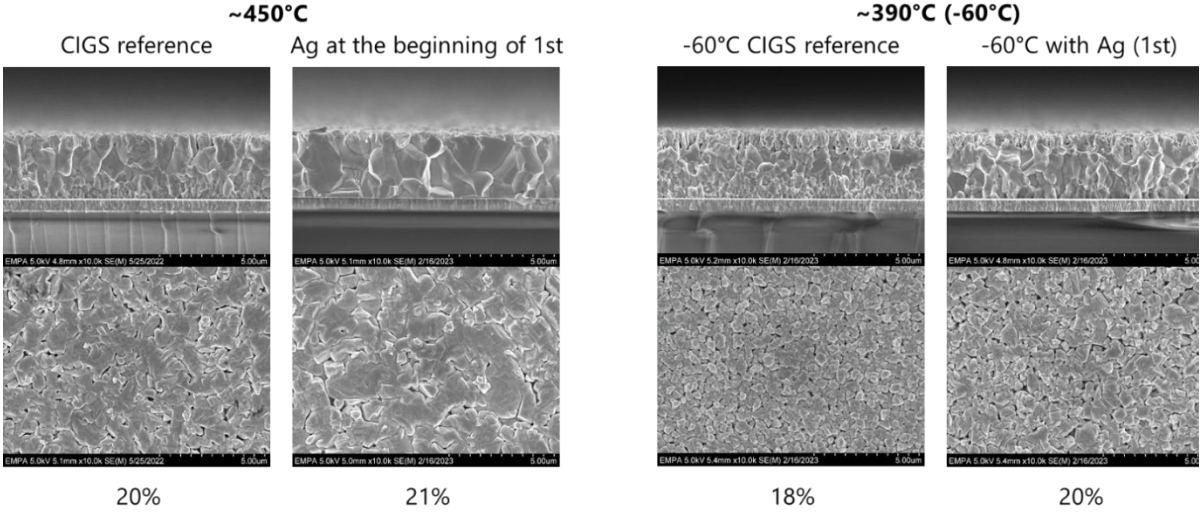

Figure 15: Comparison of the morphologies of ACIGS (AAC ~2%) and CIGS absorbers, deposited at standard and reduced temperature (-60°C nominal).

Improving the absorber morphology is an exciting feature for both direct and indirect effects on the absorber's electronic properties. First, a good morphology with large grains is favorable to higher device performance, owing to a reduction in the density of defect-containing random-orientation grain boundaries leading to a degree of non-radiative recombination and in the charge carrier scattering at inhomogeneities of the crystal affecting series resistance and FF. Second, it can also be speculated that Ag reduces the atom binding energy within the crystal, thus favoring the atom exchange between

grains and thermodynamically promoting grain growth. A lower binding energy would also help annihilate various types of point defects or extended crystallographic defects, which can impact both minority carrier lifetime and majority carrier (doping) density.

Optoelectronic properties

The absorber doping was investigated using capacitance-voltage C-V profiling for part of the samples in Table 2. Figure 16 reports the apparent C-V as a function of apparent depth. The ACIGS absorbers benefit from a high doping density close to 1e17 cm^{-3}, which we link to the excellent V_{OC} obtained. The CIGS absorbers suffer from comparatively lower values of about 1e16 cm^{-3}. A slight decrease in apparent doping density is observed when deposition temperature decreases, yet remains clearly above >1e16 cm^{-3}.

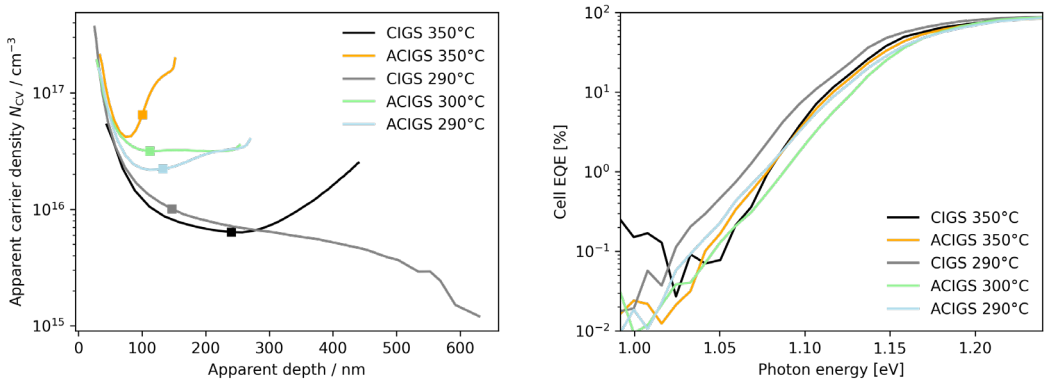

Figure 16: (left) Capacitance-voltage profiling of the apparent doping density as a function of the apparent depth for CIGS and ACIGS absorbers grown at different nominal temperatures. The ACIGS devices have higher doping levels than the CIGS ones and maintain a higher doping level at low deposition temperatures. (Right) Falling edge of EQE data in a logarithmic plot. The sub-bandgap exponential decay tails gave characteristic energies between 14 and 18 eV. Slightly sharper decays can be observed with low-temperature deposition processes.

The electronic disorder within the absorbers was explored using external quantum efficiency, specifically the exponential tail below the bandgap. Values between 14 and 18 meV were obtained for the characteristic energy, which is a signature of the magnitude of the disorder, independently from the nature of the mechanism at play (composition fluctuations, fluctuating electrostatic potential in the presence of traps, tunnel-assisted recombination near defects, etc.) CIGS and ACIGS behave similarly; both absorbers feature slightly degraded values with lower deposition temperatures, however without becoming a limiting factor for device performance. In a previous work using SLG substrates, we identified a dramatic increase for CIGS, at temperatures slightly the ones investigated here, while ACIGS behaved in a more resilient manner.

Finally, the voltage losses were investigated by means of absolute photoluminescence quantum yield. Measurements were conducted on the investigated sample series, after removal of the top transparent conductive oxide (TCO) for proper measurement conditions without extraction of charge carriers. The photoluminescence quantum yield (PLQY) value depends on the share of radiative to non-radiative recombination events in the absorber, with higher values indicating higher internal voltages inside the absorber, and therefore allowing high device open-circuit voltages and device performance. A ratio of a decade between two PLQY values suggest a difference in open-circuit voltage of nearly 60 mV. To better understand the voltage losses, the absorber bandgap were extracted from the EQE of the cells according to the Tauc plot method. Then, the Shockley-Queisser open circuit voltage limit was looked up. The non-radiative voltage losses deduced from PLQY measurements is then subtracted and compared to the actual device voltage. Experimental considerations prevent the interpretation of deviations smaller than 10-20 mV. The values are reported in Figure 17. The ACIGS absorbers grown

at standard temperature performed best, followed by CIGS grown at high temperatures and ACIGS deposited at reduced temperatures. All samples offer an excellent agreement between predicted value based on PLQY measurements, and actual device V_{OC}. A lower values of the device V_{OC} would hint at a defective interface, or voltage transport losses. None of the samples investigated appear to be limited by interface recombination.

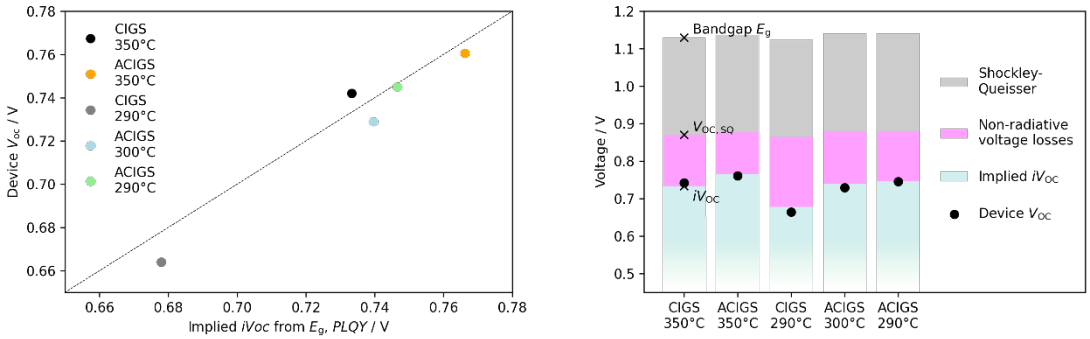

Figure 17: (left) Comparison of devices open circuit voltage (vertical axis) and implied iVoc calculated as the Shockley-Queisser voltage limit corresponding to the bandgap energy extracted from EQE, subtracted from the non-radiative losses calculated from photoluminescence quantum yield measurements. The black line shows equality of the two quantities. A very good match between predictions and actual device voltage is obtained, within the level of confidence we can ascribe to the method. (Right) Visual representation of the different voltage loss mechanisms considered, showing their respective importance.

Processing limits

A processing limit encountered when investigating Ag-alloyed specifically deposited at low temperatures is the difficulty of detecting the stoichiometry point by a thermal method. The evaporation rates of the Cu, Ga, and In evaporation sources constantly fluctuate over time, up to few percent in between consecutive runs. The final composition of the absorber and the process reliability can be improved in a laboratory environment by detection of the stoichiometry point, i.e., the moment at which equal amounts of group-I (Cu, Ag) and group-III elements (Ga, In) have been evaporated on the surface. In the case of CIGS, the detection is possible by the formation of parasitic $CuSe_x$ phases segregating on the surface, which affect the sample's thermal emissivity and its temperature in a detectable manner. The CIGS evaporation process designs this point late in the deposition process for better absorber quality and controllability of the final composition. The challenging detection of this stoichiometric point for Ag-alloyed absorbers deposited at very low temperatures (290°C nominal and below) complicates the investigation in the lab. Its significance in industrial environments is, however, very minor. The large size of industrial coaters typically allows the implementation of one or several in-situ XRF composition monitoring tools, which provide more extended information than thermal stoichiometry point detection. Therefore, this processing limit has little to no impact on industrial deployment.

The impact of Ag alloying on substrate adhesion was also investigated. The adhesion generally increases when the grain size decreases. We indeed observed slight variations in the adhesion, noticeable to experienced operators during mechanical scribing; however, they were unlikely to affect the results of, e.g., statistical tape tests. We evaluate that the deposition temperature and presence of Ag alloying are relatively minor factors contributing to substrate adhesion. The impacts of back contact preparation, oxidation level, and Se flux during the early stages of the absorber co-evaporation are considerably more critical.

2.2.2 Task 2.2 Back contact formation

$MoSe_x$ interlayer formation

The spontaneous formation of a $MoSe_2$ interlayer enable a good quasi-Ohmic contact between Mo back contact and CIGS absorber. A concern is that with Ag precursor layer method, the formation of MoSe2 may be hindered in early stage, which could be harmful to device performance and to the adhesion to the substrate. To investigate the MoSex layer formation, we delaminated absorbers and characterized the back interface with Raman spectroscopy, for different CIGS and ACIGS absorbers grown at different temperatures on Mo/glass substrates (see Figure 18). $MoSe_x$ is a layered compound, and the layer thickness can be evaluated from the Raman peak shift iv. For all samples we observe a clear MoSex signal. The presence of the Ag precursor layer does no significantly affect the MoSex layer thickness; by contrast the processing temperature has a stronger impact. We note that we investigated layers grown under standard laboratory conditions containing rather thin $MoSe_x$ interlayers: the findings must be confirmed with processing conditions more representative of industry, with thicker $MoSe_x$ layer providing strong substrate adhesion.

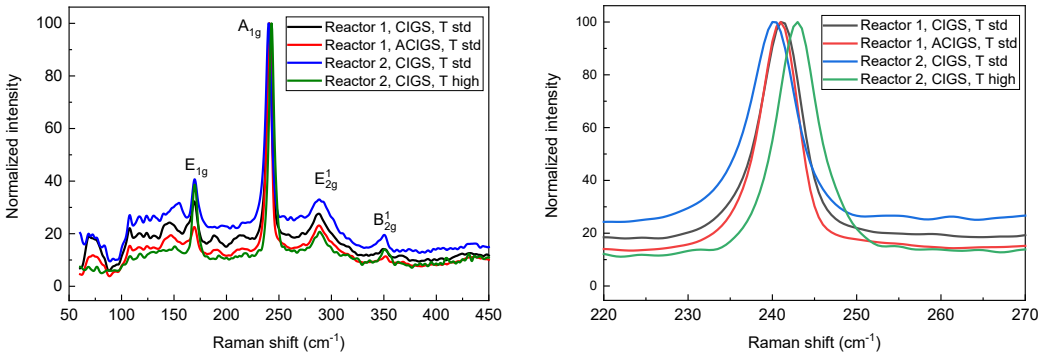

Figure 18: (left) Raman spectra of delaminated CIGS/$MoSe_x$ after delamination from the substrate. $MoSe_x$ layers was detected on all samples. The peak shift can be interpreted as the thickness of the $MoSe_x$ interlayer. The processing temperature "std" is compatible with polyimide substrates, "high" is about 80 K higher. Temperature influences the film formation, and the presence of the precursor layer has a smaller impact, at least with the processing conditions leading to formation of relatively thin layers. (right): close-up showing the peak shift.

Substrate adhesion

Cu(In,Ga)Se_2 (CIGS) alloying with Ag alloying greatly increases the grain size in absorber layers. When implemented either by the metal precursor layer approach evaporation or at the onset of the CIGS co-evaporation process, the metal does cover the Mo back contact, possibly affecting the formation of the $MoSe_x$ interlayer and the adhesion to the substrate. A lower substrate adhesion may be detrimental to the commercial prospects of products based on the new alloyed layers. In the following, we assess the risk that modified absorber composition may affect the substrate adhesion.

We tested the adhesion to the substrate by comparing CIGS and (Ag,Cu)(In,Ga)Se_2 ACIGS absorbers deposited on back contacts with and without an additional MoO_x adhesion-promoting layer onto the Mo-coated SLG substrate. Upon exposure to Se, the MoO_x material readily transforms into $MoSe_x$, which strongly increases the absorber adhesion. Our standard laboratory process results in weak adhesion to the substrate. With this experiment, we assess whether the Ag alloying influences the absorber's adhesion to the substrate.

MoO_x adhesion-promoting layers were deposited on top of the Mo back contact by reactive sputtering. The thickness was about 10 nm. CIGS and alloyed ACIGS layers were deposited using the processes described in D1.1. After deposition, the samples were subjected to the following tape test: a thin

scratch was induced in the (A)CIGS layer by mechanical scribing, then a tape was applied and subsequently removed. The scratch acts as a weakness, prompting delamination during the tape test.

The results are presented in Figure 19. Adhesion to the substrate was significantly improved upon deposition of the adhesion promoter MoO_x layer, as no delamination was triggered at the scratch location. We noticed no significant difference between CIGS on the one side and Ag-alloyed ACIGS absorbers obtained for either co-evaporation or precursor methods on the other side. Although difficult to quantify, the perception of the operator conducting mechanical scribing confirms that the adhesion promoter layer is effective and that CIGS and ACIGS absorbers had comparable adhesion to the substrate. We conclude that deposition of MoO_x effectively increases adhesion for both CIGS and ACIGS in a very similar manner and that similar adhesion is expected for both Ag incorporation methods, precursor, and co-evaporation.

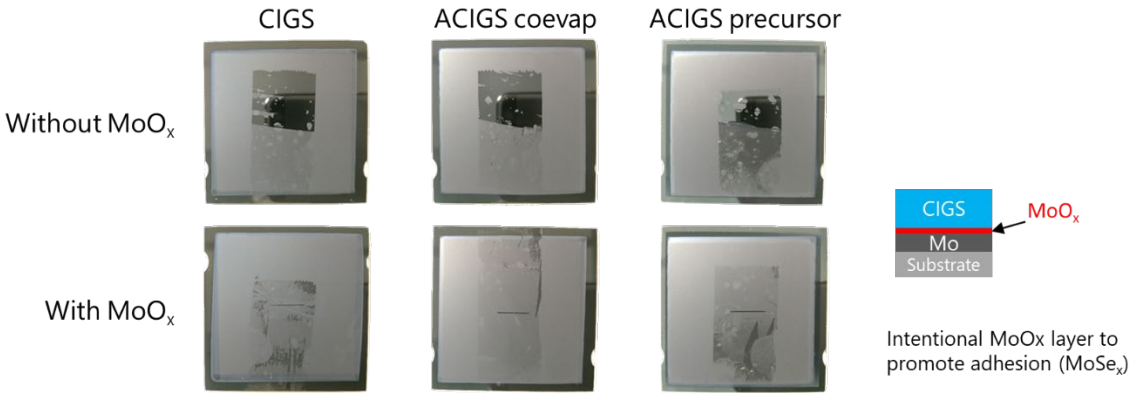

Figure 19: Cartoon of the investigated sample layer stack and results of delamination tests.

2.2.3 Task 2.3 Simple, fast and robust deposition processes

The intricate procedure developed in the lab for record efficiencies is difficult to scale-up and it is crucial to quantify the expected performance losses with simplified processes. We explored simplification of the alkali processes, simplified substrate temperature management, as well as accelerated deposition rates.

Simplified alkali processes

To develop fast and robust deposition process, we compared the influence of Ag alloying (AAC~ 2%) on PV performances while performing different simplifications to the baseline process shown in Table 3. We reduced the number of incorporation steps for alkali elements from 4 (2 for Na, 2 for Rb) down to 0, for both CIGS and ACIGS absorbers. Table 3 summarizes the cell efficiencies achieved with different alkali treatments, on absorbers with and without Ag. The values are of typical devices, without anti-reflective coating (ARC) and without heat-light soaking treatment (HLS) unless specified otherwise. It must be recalled that statistics is still limited for some variations, and that optimization was only conducted for the most complex alkali incorporation strategies.

When comparing CIGS and ACIGS devices, the typical largest change is an increase in V_{OC}. The improvement is also observed in absence of alkaline process. The reason for V_{OC} improvement may relate to the increase in doping density, and possibly in carrier life time for non-optimized alkali treatments.

Table 3: Summary of the influence of Ag alloying (AAC~2%) on PV performances of typical devices, in relation to the alkali treatments. Performances are without (ARC) and without heat-light soaking treatment unless indicated otherwise. The J_{SC} and FF values are omitted because of lack of variations. Except for alkali-free devices, all devices show FF values >0.75.

Na	Rb	CIGS	ACIGS	Performance gain with Ag
none	none	SLG substrate CGI 0.88, GGI 0.40 Eff 12.6 % V_{OC} 569 mV	SLG, coevaporation AAC 0.02, CGI 0.89, GGI 0.39 Eff 13.9 % V_{OC} 588 mV	Limited number of devices V_{OC}, FF improved
NaF PDT	None	SLG CGI 0.91*, GGI 0.39 Eff 18.0 % V_{OC} 700 mV	SLG, coevaporation AAC 0.02, CGI 0.92, GGI 0.39 Eff 18.4 % V_{OC} 708 mV	V_{OC} may be slightly improved
NaF PDT	RbF PDT	PI CGI 0.93 +, GGI 0.41 Eff 18.9 % V_{OC} 696 mV	PI, precursor AAC 0.03, CGI 0.92, GGI 0.42 Eff 20.2 % V_{OC} 736 mV	Mainly Voc improved
NaF PDT & during 3rd stage	RbF PDT	PI (best) CGI 0.99, GGI 0.42 Eff 20.1 % V_{OC} 733 mV	N/A	N/A
NaF PDT & during 3rd stage	RbF PDT & in cap	PI substrate Eff 20.6% V_{OC} 742 mV	PI, coevaporation Eff 21.1% V_{OC} 761 mV PI, precursor Eff 20.6% V_{OC} 764 mV	V_{OC} improved
NaF PDT & during 3rd stage	RbF PDT & in cap	Certified (ARC + HLS) PI substrate Eff 21.38% V_{OC} 746.7 mV	Certified (ARC+HLS) PI, coevaporation Eff 22.19% V_{OC} 763.8 mV PI, precursor Eff 22.14% V_{OC} 764.7 mV	V_{OC} improved

* best CGI composition for CIGS with NaF-PDT is around 0.85
\+ best CGI composition for CIGS with NaF+RbF PDT is around 0.90

Differences can also be seen between different alkali treatments. With NaF-PDT only, device efficiencies remain low and the improvement brought by Ag seems only marginal. On the other hand, when adding RbF PDT, the effect of Ag on V_{OC} is clearly apparent. This could be a hint to consider to acquire deeper understanding of the impact of Ag alloying. At this stage of the project, it appears that the benefits of Ag alloying may only become significant when the absorbers are treated with a combination of Na and heavier alkali elements (Rb).

For any given alkali incorporation procedure, silver improves the device efficiency by about 1%. With further application of ARC and heat-light soaking treatment, high device efficiencies >21% on flexible PI substrates appears within reach, with a simplified process with a single incorporation step for both

Na and Rb elements.

Simplified temperature profile and group-I deficiency

In a subsequent experiment, evaluated the simplification of the temperature ramps during processing, and explore the robustness of the process with absorber compositions far from stoichiometry. Instead of increasing the temperature during 2nd stage and decreasing it for the alkali processing step, we conducted depositions at constant temperature throughout the process as illustrated in Figure 15. The simplified temperature profile was used to produce absorbers with several degree of group-I deficiency. Near-stoichiometry absorbers benefit from better optoelectronic quality and generally perform better; however, absorbers with group-I excess suffer from segregation parasitic phases very detrimental to device performances. Formation of such phases must be avoided, hence compositions significantly below stoichiometry may be preferred in manufacturing environment. Absorbers with I/III ratios of 0.95 (near-optimum) yielded power conversion efficiency above 20%, while the ones with reduced I/III of 0.84 performed better than 19%. These values compare favorably with CIGS devices obtained with standard temperatures, with performance at least as good and similar performance decline with reduced composition ratio. We conclude that simplified temperature ramps are possible. The decline in device efficiency is essentially related to the lower effective temperature during the 3rd stage.

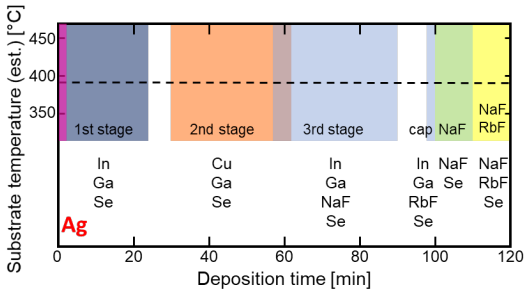

Figure 20: (left) Schematics of a simplified ACIGS deposition process with simplified temperature management.

Accelerated rates and simplified Ga deposition sequence

Since we already reported modified 3-stage absorber deposition processes with fast 1st and 2nd stages v, we here focus on accelerated deposition rate in 3rd stage, which is known to be the most critical to the performance of CIGS solar cells. We shortened the 3rd stage duration from 30 min to 8.5 min. Accelerating the deposition speed affects the elemental interdiffusion, therefore the compositional grading. Therefore, we also modified the process by skipping Ga during the 2nd stage, and adjusted the Ga rate accordingly during the 3rd stage, to help realizing the desired GGI grading with a low temperature CIGS preparation process. Both Ag-free CIGS and Ag-containing ACIGS absorber compositions were evaluated.

As the result, the process developed does qualify as accelerate deposition process, as well as simplified process as Ga deposition is not anymore needed in the 2nd stage.

Figure 21(left) compares cross-sectional SEM images of ACIGS and CIGS layers by accelerated processes to devices obtained with the standard process. Ag-containing ACIGS feature comparable morphology regardless of 3rd stage acceleration. By contrast, in absence of silver the accelerated process leads to the presence of smaller grains at the surface area. The deposition parameters most effectively acting on the grain growth near the front surface are the maximum compositional group-I excess ACGI ratio achieved, and the process duration under Ag-Cu excess condition (over stoichiometry). Increasing the ACGI and extending the Ag-Cu excess duration yields large grains. In the developed accelerated process, both are reduced from 1.15 down to 1.07 (ACGI) and 24 min

down to 7 min (duration). While the morphology is significantly degraded with CIGS composition, alloying with silver is very effective at maintaining a suitably good morphology.

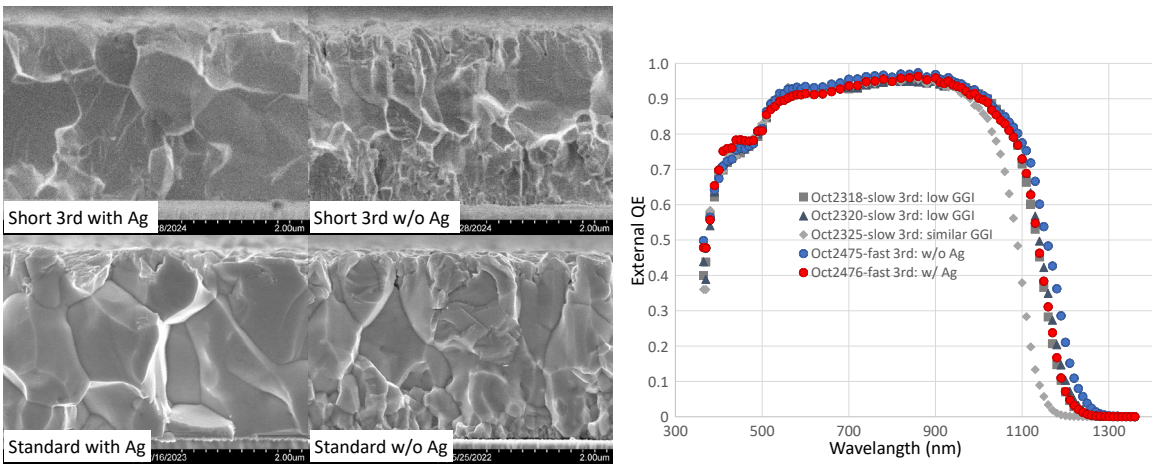

Figure 21: (left) Cross sectional SEM images for ACIGS and CIGS layers prepared with the accelerated and standard processes. (right)

Figure 21(right) shows the EQE curves of the samples with slow and accelerated depositions, illustrating how the gradient and optical bandgap are affected by the growth rate. PV performances of samples prepared by developed process feature a lower V_{OC} than to samples prepared by standard process with similar depth-integrated composition ratio GGI. For the most part, this is attributed to the change in GGI grading and corresponding change in the band gap minimum stemming from the absence of Ga in 2nd stage. Restraining comparison to solar cells with similar bandgap, ACIGS cells prepared with the accelerated process have same PV properties efficiencies as to the ones prepared by standard processes. ACIGS cells clearly have better performances than Ag-free CIGS ones. The ACIGS device with accelerated process also presents a comparable Voc deficit as compared to standard process. PLQY (ΔV_{OC_PLQY}) measurements quantify the V_{OC} drops caused by non-radiative recombination in the bulk to 97 meV for ACIGS (comparable to our best cells), and a more unfavorable value of 115 meV loss for CIGS by accelerated process.

With accelerated deposition rates, alloying with silver enables faster grain growth and results in high quality absorber layer as compared to CIGS composition. With device efficiency up to 20.5%, ACIGS solar cells with high deposition rate show the same PV performance as cells with slow rates and comparable bandgap.

2.3 WP 3 Mini-modules and device stability

2.3.1 Task 3.1 Mini-module development by laser patterning for interconnections

This task assesses the feasibility of processing modules with the new, Ag-alloyed ACIGS absorber layers for module-making in view of the potential transfer of the process to industry manufacturers. The impact of absorber modifications is discussed on the different scribe lines necessary to complete the active flexible foils into solar modules.

The power conversion efficiency of solar modules is generally lower than that of individual solar cells because of several reasons. The module area comprises regions not covered by active solar cells: the inactive regions are called "dead area". Requirements for lateral conductivity are more stringent for modules than for lab-scale solar cells, which affects the optical transparency of the window layers, such as the free carrier absorption in the top transparent conductive oxide (TCO). The electrical interconnections are also a source of electrical losses: adjacent solar cells must be electrically insulated from each other, and a low-resistance electrical path must connect the front contact of one cell to the bottom contact of the adjacent one.

Figure 22 shows a schematic representation of the monolithic cells interconnection. Ideal P1 and P3 are perfectly insulating and P2 perfectly conductive. Non-negligible parasitic resistive or conductive paths appear in real PV modules, causing a non-ideal FF.

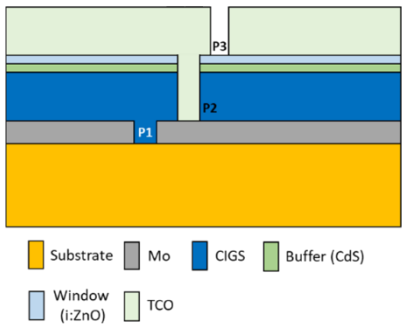

Figure 22: Schematic representation of the monolithic interconnection process.

Front TCO

Before considering scribing processes, we selected and compared two variants for the top TCO electrode, aiming at sheet resistances of about 10-20 Ω□:

A single, 750 nm thick ZnO:Al (AZO) layer. AZO is a comparatively cheap material that provides best performance at solar cell level. However, carrier mobility is typically limited to about 20 $cm^2/V/s$, such that thick layers or high doping levels are required for sufficient lateral conductivity leading to significant free carrier absorber and reduced Jsc.

A bilayer structure with a 50 nm thin AZO layer for electrical contacting to the cell and a thicker, 35 nm InZnO (IZO) layer with better performance ensures lateral conductivity. The second option yields Jsc improvement by about 2 mA/cm2 as compared to thick AZO layer only and is therefore preferred for module making.

P1 scribe lines

The P1 scribe insulates the bottom contact of adjacent cells, which consist of metal Mo layers. Scribe parameters were optimized to reach good insulation without damaging the PI substrate. Assuming effective physical separation of the metal areas, the insulation capability of the scribe is limited by

conductivity of the semiconductor absorber material mediated by majority carriers. The conductivity therefore relates to its width as well as the doping level in the absorber layer: larger widths and low doping levels are beneficial. P1 becomes limiting with the modified, Ag-containing ACIGS absorbers with high doping level. However, a larger width also reduces the geometrical fill factor and the device active area, hence lowering the module efficiency. Different P1 widths were investigated to insulate the bottom contact without excessively reducing the active area.

The optimal width for the fabricated modules was found to be 130 µm, achieved by patterning of several parallel lines. The P1 scribe was performed through the substrate.

P2 scribe lines

The P2 conductive scribe connects the top contact of one cell to the bottom contact of the adjacent one. The P2 process was optimized to achieve the highest possible conductivity and minimize the scribe width. A continuous wave laser was used to melt the layer stack and connect top and bottom contacts. A discontinuous line design was chosen for the scribe; the optimal dimension of each dot was found to be 0.1 mm in length, with a spacing of 0.1 mm. The scribing parameters resulted in a scribe width of 100 µm. The specifics of the TCO top electrode were found to affect the quality of the P2 scribe.

- With thick AZO, the TCO layer with thickness of 750 nm was deposited with a one step process, followed by P2 scribing step.
- With highly transparent InZnO (IZO), the best processes were obtained with a two steps deposition approach. First, a 50 nm layer of AZO was deposited, followed by the P2 scribing step, then the thick IZO layer of 350 nm was deposited.

P3 scribe lines

The P3 insulation scribe removes the top TCO between adjacent cells. Several processes were evaluated to maximize the P3 line resistance. Since TCOs are almost transparent at infrared wavelengths, a 1064 nm wavelength laser typically removes the TCO by explosively ablating the near-surface of the underlying CIGS absorber layer. However, this process can damage the CIGS surface, leading to the formation of parasitic shunt paths and reduce the module Rp and FF. While the results for AZO contact offered satisfying quality, scribing of IZO was limiting the device performance.

The thick AZO layers could be scribed with a 1064 nm NIR laser with good performance, with a scribe width of about 100 µm.

For IZO/AZO bilayers, we investigated P3 scribing with a 355 nm laser instead of a 1064 nm one. In contrast to infrared lasers, UV lasers depose a high percentage of power (≈78 %) in the TCO layer itself instead of in the underlying layer, which mitigates thermal damage to the CIGS surface and limits the formation of parasitic shunt paths. The best identified process for IZO with the UV laser was achieved with a width was 116 µm.

As a third possibility, we also explored to realize the P3 scribe by mechanical scribing, by mechanically peeling off the CIGS absorber from the Mo substrate, in a similar manner as performed for the delimitation of lab-scale solar cells.

PT module delimitation scribe

The PT scribe delimits the sides of the modules. This is a standard and straightforward process in the industry and is not critical for large-area devices. However, with our small-scale devices of few cm^2, the PT scribe is much more important. We first tried to combine one P1 and two P3 scribes using the

recipes already developed, but the results were not satisfactory. Consequently, similarly to the P3 scribe, mechanical scribing was used to ensure isolation.

Module performance

The best processes presented above were implemented to fabricate PV mini-modules on flexible polyimide with 5 subcells. In addition to JV curves, lock-in thermography analyses were carried out to determine the cause of the shunting losses. Lock-in thermography is a very sensitive technique to identify the location of shunts by detecting their change in thermal radiation due to Joule heating.

The JV curve of the module with AZO top electrode and mechanical scribing is presented in Figure 23(A), The PV parameters are: V_{OC} 3.5 V, J_{SC} = 6.98 mA/cm2, FF 61.2%, and PCE 15.0%. The average cell performance of the reference layer is 17.6%, which correspond to a cell-to-module loss of 2.6% absolute. From Figure 23(B), the main contributor to device shunting are the PT scribes. The process left an unacceptable number conducting defects. An optical microscopy inspection of the relevant locations revealed that the shunts were caused by residual absorber present in the P1 trench, which were not fully removed during the mechanical scribing.

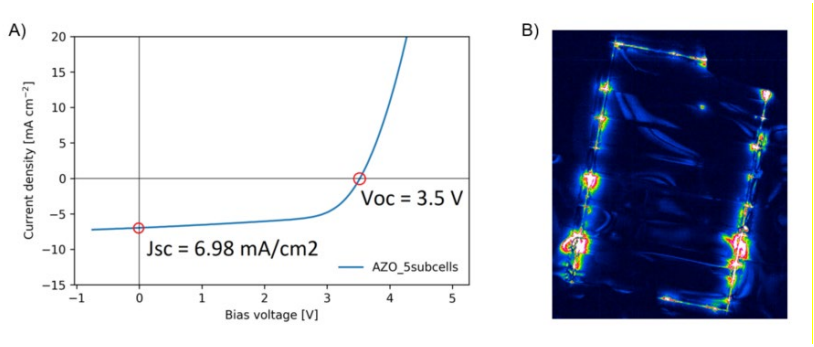

Figure 23: A) Flexible mini-module fabricated on flexible PI film with AZO top contact; B) Lock-in thermography image of the mini-module after mechanical scribe of P3 and PT.

Figure 24(A) presents the electrical response of minimodule made with IZO/AZO bilayer TCO as top contact and comprising 5 subcells. The P3 scribe was performed mechanically. We achieved 3.41 V Voc, 6.9 mA/cm^2 Jsc, 59.0% FF, and 13.87% power conversion efficiency. The average performance of cells of the reference absorber with identical layer stack is 16.5%, which correspond to a cell-to-module loss of 2.63%. The thermography image in Figure 24(B) shows the main contributor to device shunting is located along the PT edge scribe lines. In addition to the shunts at the edges, a hot spot is also visible in the active area (bottom-left quadrant).

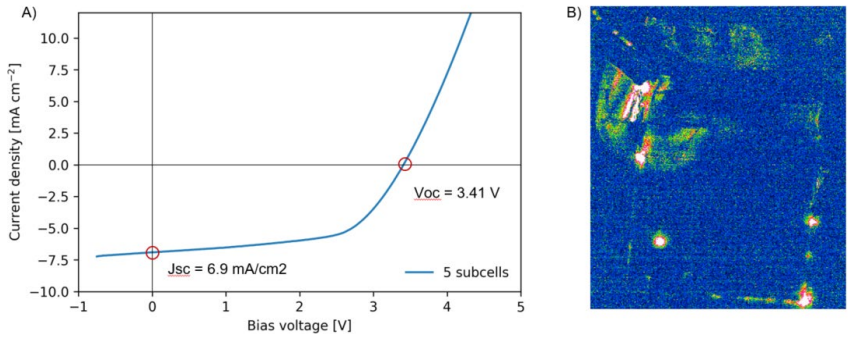

Figure 24: (A) Flexible mini-module fabricated on flexible PI film with thin AZO/IZO top contact; (B) Thermography image of mini-module after mechanical scribe of P3 and PT.

Table 4 compares the JV parameters of the minimodules and the reference cells. Jsc is slightly increased from cell to module, which is partly caused by the shading losses in the reference cell due to the presence of the grids. The Voc is essentially maintained; the main issue is the FF loss which primarily stems from shunting issues at PT scribes.

Table 4: JV parameters of minimodules and reference cell

Device	Jsc mA / cm^2	Voc V	FF %	Efficiency %
Minimodule AZO	6.98	3.5	61.2	15.0
Minimodule AZO (per cell	34.9	0.700	61.2	15.0
Minimodule IZO/AZO	6.9	3.41	59.0	13.9
Minimodule IZO/AZO (per cell)	34.5	0.682	59.0	13.9
Reference cell IZO/AZO	32.79	0.693	72.6	16.5

In this module the edge insulation was performed by combination of P1 and P3 lines, followed by mechanical scribing to improve isolation. The development of a better performing recipe would improve the quality of the edge insulation thereby entirely avoiding the need for mechanical scribing. Also, while for our small-scale mini-module demonstrators the PT scribes deserve further improvements, for upscaling to industrial production the lateral scribe is less critical.

The current P1 process is believed not optimal, although its impact is small in comparison to the edge insulation discussed above. The high doping level inside the absorber (usually 10^{16} - 10^{17} cm^{-3} in ACIGS absorbers) limits the isolation performance. A possible solution would be the complete removal of the absorber followed by the deposition of an insulating material inside the scribe to ensure isolation; this would improve the P1 performance, and the same technique could also be used to tackle the issues with the PT scribe discussed above. While this method would add one additional step to the whole fabrication process, it would allow performing the P1 scribing step after the absorber deposition, potentially at the same time as the P2 scribe.

A further loss mechanism can be inferred from the JV curves, relates to the device apparent series resistance. This increase in series resistance could be evaluated to originate from two origins about equally contributing: the sheet resistance of the front TCO, and sub-optimal P2 process. Implementation of a more classical P2 process by complete removal of the absorber thickness (instead of the melted dash approach) should improve the device performance.

2.3.2 Device performance stability

Shelf degradation

The first, basic assessment of the device stability regards the performance stability of ACIGS solar cells when stored in ambient, indoor condition. The shelf life degradation was found negligible over time scales of months.

Accelerated testing

CIGS solar cells, Ag-containing solar cells, and an ACIGS minimodule we subjected to accelerated stress tests consisting of >1000h cumulated duration at 85°C in 0.5 atm N2 under 1-sun illumination. The devices were maintained in open circuit condition. The change in device performances were evaluated ex-situ at regular intervals during the stress procedure. The devices layer structure was:

- cells: Al:ZnO / iZnO / CdS / (A)CIGS / Mo / PI
- module: InZnO / Al:ZnO / iZnO / CdS / (A)CIGS / Mo / PI. P3 by mechanical scribing.

Figure 25 shows change in PV parameters of CIGS and ACIGS solar cells (average of the cell performance in the sample), as well as of a ACIGS mini-module. After 1000h under stress condition, no degradation was observed, rather, a slight improvement in the device efficiency was found, driven by voltage and FF. This improvement is known as heat light soaking. Most of the improvement occurs during the first 24h. The ACIGS solar cells show a larger improvement than Ag-free CIGS cells and maintained their improved state until the end of the test after 1000 h.

In comparison, the CIGS cells performance started to degrade almost back to their initial state after about 400h. It must be noted that the degradation of CIGS cells after 200h resulted from an inhomogeneous degradation of cell performance through FF, and a few cells maintained their improved state.

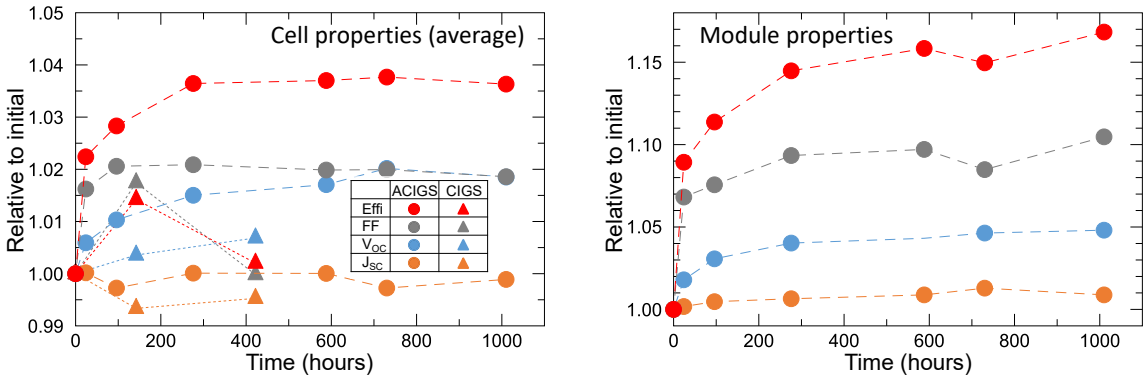

Figure 25: (left) PV properties of solar cells (average of cells the sample) during the accelerated stress test. (right) PV properties of the mini-module. Samples were taken out from the stress chamber to measure the PV properties after certain durations under stress condition. After measurements, the samples were placed back into the stress chamber and the stress was resumed.

The improvement in PV performance of module is much greater than that of individual solar cells, primarily through a drastic improvement in the FF. The primary reason is because the minimodule initially suffered from much reduced FF (slightly below 60%) due to device shunting. Upon stress conditions the FF quickly improved by 6%, which we attribute to healing of defects at the scribing lines.

The voltage correspondingly improved when the device shunting was mitigated. Further voltage increase is observed over time, seemingly comparable to the voltage increased observed in individual solar cells. Importantly, the minimodule did not degrade over time.

In conclusion, the ACIGS solar cells improved performance by about 3 to 4% driven by voltage and FF, most of the gain being acquired during the first few hours of testing. The Ag-alloyed ACIGS solar cells present better stability than CIGS ones. The tested minimodule improved its performance upon stress, driven by mitigated shunt at the scribe lines and resulting improved FF, obtained in the beginning of the stress test. We demonstrate the excellent stability of the ACIGS solar cells and modules.

2.4 Related developments

2.4.1 Absolute photoluminescence tool

During the last months we build, set up and started to routinely use a home-made setup to measure the photoluminescence quantum yield PLQY of absorber and devices. The purpose of the instrument is to predict open-circuit voltage at an early stage, understand the non-radiative recombination mechanisms, and discriminate between bulk and interface recombination by combining information at different processing stages and in combination with other methods (TRPL, C-V). The technique is a good candidate for in-line integration in a production line.

Commercially available setups typically feature a Si detector, limiting its use for CIGS and related compound due to the operating wavelength range. If not, the sensitivity is also typically limited to PLQY values down to the percent range or only slightly better. The setup must also be easily accessible and operable within minutes for routine measurements.

The schematics and a picture of the optical setup is provided in Figure 26. The excitation is provided by a chopped 640 nm laser light guided through a fiber and projected by a pair of lenses onto the sample into a 2 mm diameter disk. The very simple optical configuration for light collection consists of a pair of parabolic mirrors collecting and directing the emitted light onto a Ge photodetector, and a spectral filter. The mirrors are preferred for quantitative measurement as no chromatic aberration is induced, although their spectral response has to be taken into account. The detector area is about 1 cm^2 to accommodate the large excitation spot size and the spot deformation by the mirrors. The electrical detection is performed by a lock-in amplifier. PLQY values down to the 1e-7 range can be detected, and the setup is sensitive over the wavelength range 700-1700 nm.

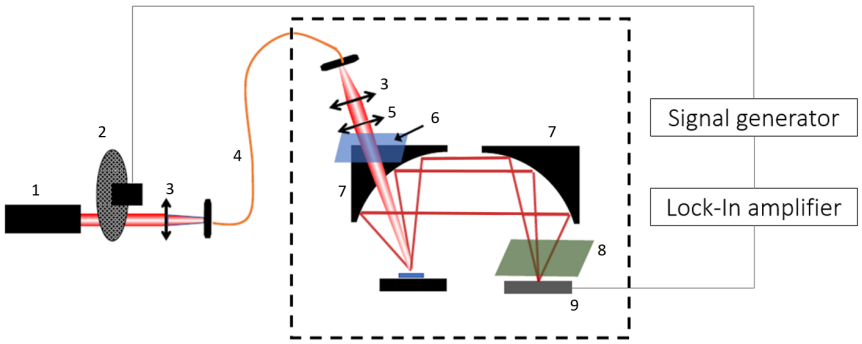

Figure 26: Schematics of the developed PLQY setup. See text for a detailed description.

The setup is now routinely used. Some of the obtained results are reported in section 2.2.1. As compared to the system sketch in Figure 26, a further development has been implemented consisting in a power dependency control and monitoring. This system enables the investigation of the optical diode behaviour, to understand and predict the device FF. In the longer term, spectrometry could be included with e.g. coupling to a spectrometer or integration of a tuneable bandpass filter.

3 Conclusions and outlook

The project ACIGS met its objectives, conclusively demonstrating the advantages of silver alloyed ACIGS absorbers over legacy CIGS ones and delivering clear insights about how the processes can be ported to industry production lines.

This section summarizes our main findings and is structured according to the main project objectives.

Demonstrate the technology potential:

- Incorporating a low amount of silver (2% Ag versus Cu) into CIGS absorbers improves the photovoltaic performances by about 0.5-1% absolute.
  The performance increases stem from a 10-20 mV Voc increase, originating from an increase in the absorber doping level.
- We demonstrate record CIGS solar cells on flexible foils with improved 22.2% power conversion efficiency (externally certified value), significant progress from the 21.4% starting point.
- With low-temperature, standard bandgap ACIGS absorbers, RbF as a precursor layer does not result in efficiency improvements. Excessive amounts degraded the microstructure, and reduced carrier density, voltage and power conversion efficiency.

A simplified fabrication process for high-efficiency flexible CIGS devices on polymer with **relaxed manufacturing tolerances** intended for reduced lab-to-fab performance gap. Low sensitivity (device performance loss < 1%) to process simplifications or to variations in parameters:

- ACIGS absorbers benefit from a performance boost over a wider range of Ga composition than CIGS. The identified process window is GGI between 0.35-0.41, and bandgap 1.12-1.16 eV.
- A reduction in the number of alkali incorporation steps from 2+2 (laboratory process) down to 1+1 (simplified process with only NaF & RbF PDT) leads to a loss in performance by 1%.
  Cell efficiencies >21% should be achievable with a simplified process featuring only NaF & RbF PDT.
- Regardless of the complexity of the chosen alkali incorporation procedures, Ag alloying improves the solar cell performances by about 1%.
- Reducing the ACIGS deposition temperature by about 60°C compared to the standard value of about 450°C leads to a degradation in PV performance by 1% absolute only, yielding similar performance as CIGS layers grown at optimal temperature.
  The performance degradation of Ag-free CIGS at reduced temperatures is about twice as severe.
- A drastic simplification of the substrate temperature is possible with <1% performance loss.
  ACIGS absorbers always outperform CIGS ones irrespective of the deficiency in group-I elements.
- ACIGS absorbers prepared with accelerated process (3rd stage & cap within 8 min vs 30 min) show the same performances as with standard process with the same optical bandgap, which is not the case for CIGS composition. Alloying with Ag makes the absorber deposition process more robust to the high growth rates of industry-type deposition processes.
- Limitation: we faced challenges related to the thermal detection of the stoichiometry point. This limited our investigations to very low substrate temperatures. No clear limit to the lower deposition temperature processing limit could be identified. From previous experience with glass substrates, the processing window for ACIGS is enlarged by about 50°C compared to CIGS. The encountered processing limit related to stoichiometry detection is not a problem in an industrial environment.

Transferability of the new process to industrial production:

- **Method**: The performance improvement of Ag-alloyed layers is obtained irrespective of the incorporation method (ex-situ metal precursor layer or in-situ co-evaporation), provided Ag is incorporated at the latest during the overstoichiometry phase of the deposition process. Therefore, the modification of an existing CIGS process can be performed either by modifying the CIGS deposition chamber or by adding a separate deposition process on the back contact, with similar expectations for improvement in efficiency. Therefore, external considerations may be prioritized in the decision-making process.
- **Amount**: The obtained benefits are demonstrated with low Ag amounts of about 2% AAC ratio. 2% is a quite minor amount, which is interesting in view of raw material costs as well as for process control. With such a small amount, control of Ag and Cu incorporation may be decoupled: existing control mechanisms of the Cu amount should remain effective, and Ag incorporation can be independently monitored within a relatively wide processing window (AAC 1-3%).
- **Alkali**: With the identified optimal Ag amount of 2% vs Cu, the optimum alkali PDT treatments are similar for CIGS and ACIGS, with a slight reduction in the optimum amount of heavy alkali RbF.
- **Substrate adhesion:** CIGS and ACIGS absorbers were found to offer very similar adhesion to the substrate. This was observed with native Mo substrate, as well as with substrates prepared with a MoO_x layer to promote substrate adhesion.
- **Minimodule demonstrators** with AZO or InZnO/AZO bilayer top contacts were fabricated on flexible substrates, with efficiency up to 15% and cell-to-module loss of below 3% absolute.
- **Accelerated stress tests**: ACIGS solar cells and modules demonstrated excellent stability to accelerated stress tests of >1000h at 85°C in 0.5 atm N_2 under 1-sun illumination. A slight Voc and FF gain was observed during the first hours of the test, and then the performance remained stable, contrary to a subset of the tested CIGS cells.
  Shunts of the modules at the scribe line are susceptible to improvement upon exposure to elevated temperatures.

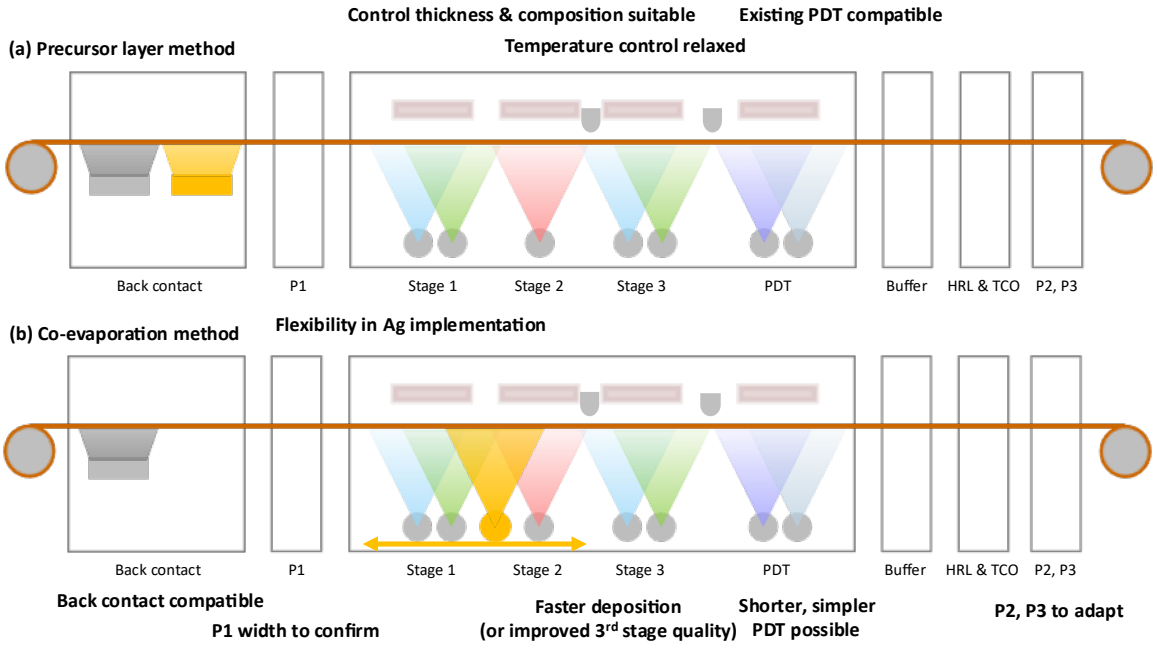

Figure 27: Blueprint roadmap for industrial process scale-up and lab-to-fab technology transfer, highlighting the main learnings of the ACIGS project.

Formalize a blueprint roadmap for industrial process scale-up and lab-to-fab technology transfer:

- Two possible routes show potential for practical implementation of the new process at an industrial scale, with very similar benefits on device performance.
  First, the equipment for back contact deposition can be modified to add an Ag metal precursor layer.
  Second, an inline CIGS evaporation tool can be modified to accommodate additional Ag evaporation sources. The sources could be placed anywhere from the entrance of the machine until the end of the Cu 2nd stage.
- Owing to the low Ag to Cu ratio, the composition control during the ACIGS deposition can be performed using existing methodologies.
- ACIGS compositions enable accelerated evaporation rate in the most sensitive 3rd stage as compared to what can be tolerated with CIGS; alternatively, improved absorber quality and performances are expected for a given rate.
- The existing alkali incorporation strategies may be used. ACIGS devices are expected to outperform CIGS ones irrespective of the specifics of the alkali treatment. The loss in efficiency with simplified alkali incorporation has been established.
- The existing back contact may be used without significant adaption.
- The monolithic interconnection strategies work for the most part, with the following adaptations.
  P3 may be preferentially performed using a blue or UV laser especially if a higher-performing InZnO TCO is used, with mechanical scribing as a back-up solution.
  Moreover, the conduction through the P1 scribe by CIGS majority carriers must be considered when the absorber doping level reaches high values beyond 1e16 cm^{-3}.

Outlook

How to push the efficiency of flexible CIGS solar cells towards 25 %

PLQY measurements indicate that the absorber non-radiative recombination is limiting the Voc. Figure 9(ERE) suggests the internal voltage is limited by a combination of two factors. First, a defect entering the bandgap at about 1.35 eV may trigger recombination in the back gradient region of the absorber and may limit the performance of high-bandgap absorbers. Second, another recombination mechanism may limit the PLQY (and ERE) to 1-2%, irrespective of the composition and bandgap. By design, the current strategy of maximizing solar cell efficiencies hits both limitations at the same time. It may be considered redirecting the efforts to absorber with either higher or lower bandgap, to tackle either of the two limitations separately. The 1.35 eV defect is probably most detrimental to single junction applications, while low bandgap absorbers have better prospects as bottom cells for tandem solar cells.

The Jsc of CIGS solar cells remains more than 10% below its Shockley-Queisser value. Optical management might enable the next efficiency leap, for example with advanced management, texturing for total internal reflection and scattering, and back reflectors. Adding bifaciality feature would also enable gains in energy yield at same efficiency levels. Empa has reported bifacial ACIGS devices with 19.8% certified efficiency value.

Finally, the FF of CIGS solar cell is limited for half, by the absorber itself through its optical diode factor (typically 1.25-1.30 for Empa absorbers, within the parameter space typically explored), and for the other half by transport and contact losses. Improving the device contacts and architecture may slightly improve the FF. Yet the absorbers produced at Empa appear limiting as demonstrated by the newly-established PLQY setup with power dependency, while there is no clear indication that this is necessarily the case for absorbers produced at other facilities/institutions.

Confidence in ACIGS manufacturing with reduced costs

While concentrating on technological aspects, we mention here ideas for research avenues that could help reduce the manufacturing costs of flexible CIGS photovoltaic technologies.

First, the research conducted at Empa historically focused on slow, lab-scale processes aiming at high efficiencies. While the ACIGS project delivered very positive insights regarding the accelerated depositions enabled by Ag alloying, demonstration of high device performance with processes closer to industrial ones may be more convincing, such as >20% efficiency with <20 min total process time.

Second, while the ACIGS project demonstrated functional minimodules with acceptable performance, it is apparent that laser patterning of state-of-the-art absorbers is more challenging than that of absorbers with inferior quality. More work is needed in that direction.

Finally, the front sheet has been a long-standing issue for flexible CIGS, and for flexible PV more generally. Typical requirements are about 1e-5 g/m2/day or below that is only possible with very expensive commercial solutions. Yet the primary failure mode concerns the degradation of ZnO and AZO front window materials. Alternative materials are possible, yet were never explored as the ZnO-based window layers are well-performing, robust, and consist of cheap materials. It is unknown whether alternative window layers may enable the use of cost-effective front sheets, reducing the manufacturing costs of flexible PV modules.

4 Bibliography

See list of references below.

---

i Green, M. A. (2012). Radiative efficiency of state-of-the-art photovoltaic cells. Progress in Photovoltaics: Research and Applications, 20(4), 472–476. https://doi.org/10.1002/pip.1147

[ii] C. Spindler, F. Babbe, M. H. Wolter, F. Ehré, K. Santhosh, P. Hilgert, F. Werner, and S. Siebentritt, "Electronic defects in Cu(In,Ga)Se2: Towards a comprehensive model", Phys. Rev. Materials 3, 090302 (2019). DOI https://doi.org/10.1103/PhysRevMaterials.3.090302
[iii] Krause et al. Solar RRL 8, 2400077, 2024 https://doi.org/10.1002/solr.202400077
[iv] Philipp Tonndorf, Robert Schmidt, Philipp Böttger, Xiao Zhang, Janna Börner, Andreas Liebig, Manfred Albrecht, Christian Kloc, Ovidiu Gordan, Dietrich R. T. Zahn, Steffen Michaelis de Vasconcellos, and Rudolf Bratschitsch, "Photoluminescence emission and Raman response of monolayer MoS2, MoSe2, and WSe2," Opt. Express 21, 4908-4916 (2013)
[v] Chirilă et.al., Prog. Photovolt. Res. Appl. 20, Influence of high growth rates on evaporated Cu(In,Ga)Se2 layers and solar cells, 209-216, 2012